University of Zurich[UZH]

Using black carbon and leaf wax lipids for improved understanding of fire traces in an archaelogical site in the Bistrița valley in Romania

GEO 511 Master's Thesis

Author
Daniela Baumann
13-703-640

Supervised by
PD Dr. Guido Lars Bruno Wiesenberg
Dr. Ulrich Hambach (ulrich.hambach@uni-bayreuth.de)

Faculty representative
PD Dr. Guido Lars Bruno Wiesenberg

30.04.2020
Department of Geography, University of Zurich

University of Zurich[UZH]

Using black carbon and leaf wax lipids for improved understanding of fire traces in an archaeological site in the Bistriţa valley in Romania

GEO 511 Master's Thesis

Soil Science and Biogeochemistry
Department of Geography
University of Zurich

April 30, 2020

Submitted by:	Daniela Baumann
Supervisor:	PD Dr. Guido Wiesenberg
External Supervisor	Dr. Ulrich Hambach, University of Bayreuth

Acknowledgements

First, I would like to thank my supervisor Guido Wiesenberg for his guidance during the whole process of this master's thesis. I greatly appreciate how well he explained things to me and I am grateful for having been given the opportunity to work with such an array of different methods. I also gratefully acknowledge the helpful inputs and provided information of my co-supervisor Ulrich Hambach. Furthermore, I want to thank Veronica Veloso and Gabriela Santilli do Nascimento for their thorough introduction into the BPCA analysis and their continuous support whenever questions or any sort of trouble arose. In this context, I would also like to thank Nicholas Otifi, who gave me many useful tips and was always open to answer questions. Additionally, I would like to express my gratitude to all the other phD students and lab technicians, who all at some point supported me with their knowledge, time and patience. Last but not least, I want to thank Patrick Paszti for the time he took to introduce me to Matlab and Latex, his constructive inputs and feedback and for his unconditional support.

Abstract

The numerous Upper Palaeolithic settlements in the Bistriţa valley in northeastern Romania have been under systematic archaeological research since the 1930s in order to unravel human cultural evolution. Despite these efforts, many questions regarding site formation and the palaeoecological context of human presence remain unresolved. The aim of this thesis was to help improve the understanding of the palaeoenvironment by analyzing traces of presumable ancient biomass burning that were discovered at Bistricioara-Lutărie III. By using a multi-methodological approach including X-Ray fluorescence, elemental analyses, lipid analyses and investigations of quantity and quality of black carbon with the BPCA (benzene polycarboxylic acid) method, it was confirmed that the dark layers in the profile were rich in charring residues. Fire horizons were characterized by significantly higher amounts of carbon, nitrogen and copper but were depleted in silicon, vanadium and chromium. The amount of black carbon in the fire horizons averaged at 89 $\pm$ 29 g kg^{-1} TOC (total organic carbon), which was significantly higher than the amount found in the bulk samples (25 $\pm$ 10 g kg^{-1} TOC). The ratio of products with 5 to products with 6 carboxyl groups (B5CA/B6CA) and other markers for estimating fire energy suggested that the fires that took place were not highly energetic, i.e. temperatures did probably not exceed $\sim$300 °C, making it very unlikely that they were campfires but rather naturally occurring wildfires. As grass can burn at low temperatures, it is plausible that it constituted an important fuel source for the fires. Lipid molecular proxies suggested that grass and herbaceous vegetation indeed made up a large proportion of the biomass during the last 35 ka. They furthermore indicated a change in vegetation composition and/or climatic conditions around the onset of the Last Glacial Maximum. The findings of this thesis have contributed to the ongoing research by drawing a clearer picture of the palaeoenvironment and humans' role in the local fire history.

Contents

List of figures

List of tables

List of abbreviations

ACL	average chain length
AMH	anatomically modern humans
ANOVA	analysis of variance
BC	black carbon
BL III	Bistricioara-Lutărie III
BPCA	benzene polycarboxylic acid
CPI	carbon preference index
DCM	dichlormethane
GC-FID	Gas Chromatography-Flame Ionization Detector
GC-MS	Gas Chromatography-Mass Spectrometry
HPLC	high pressure liquid chromatography
LGM	Last Glacial Maximum
OM	organic matter
PAH	polycyclic aromatic hydrocarbon
TLE	total free extractable lipid content
TOC	total organic carbon
V-PDB	Vienna Pee Dee Belemnite
XRF	X-Ray fluorescence

1. Introduction

Since humans' African origin was first proposed by Charles Darwin in the 19th century (Darwin 1871), the migration of anatomically modern humans (AMH) out of Africa has been of great scientific interest. Using mitochondrial DNA, researchers have estimated that AMH left the African content around 60 to 40 ka ago (Underhill & Kivisild 2007). In their review, López *et al.* 2015 point out the ongoing debate regarding the timing, the number of dispersals and the route of AMHs' exodus from the African homeland. Researches agree however that if there was only a single wave of migration, there were two possible routes: A northern route, which led through Egypt and the Sinai and a southern route passing across Ethiopia, the Bab el Mandeb strait, and the Arabian Peninsula. These options are not mutually exclusive (López *et al.* 2015). In any case, AMH entered Europe through Eurasia and Eastern Europe (fig. 1).

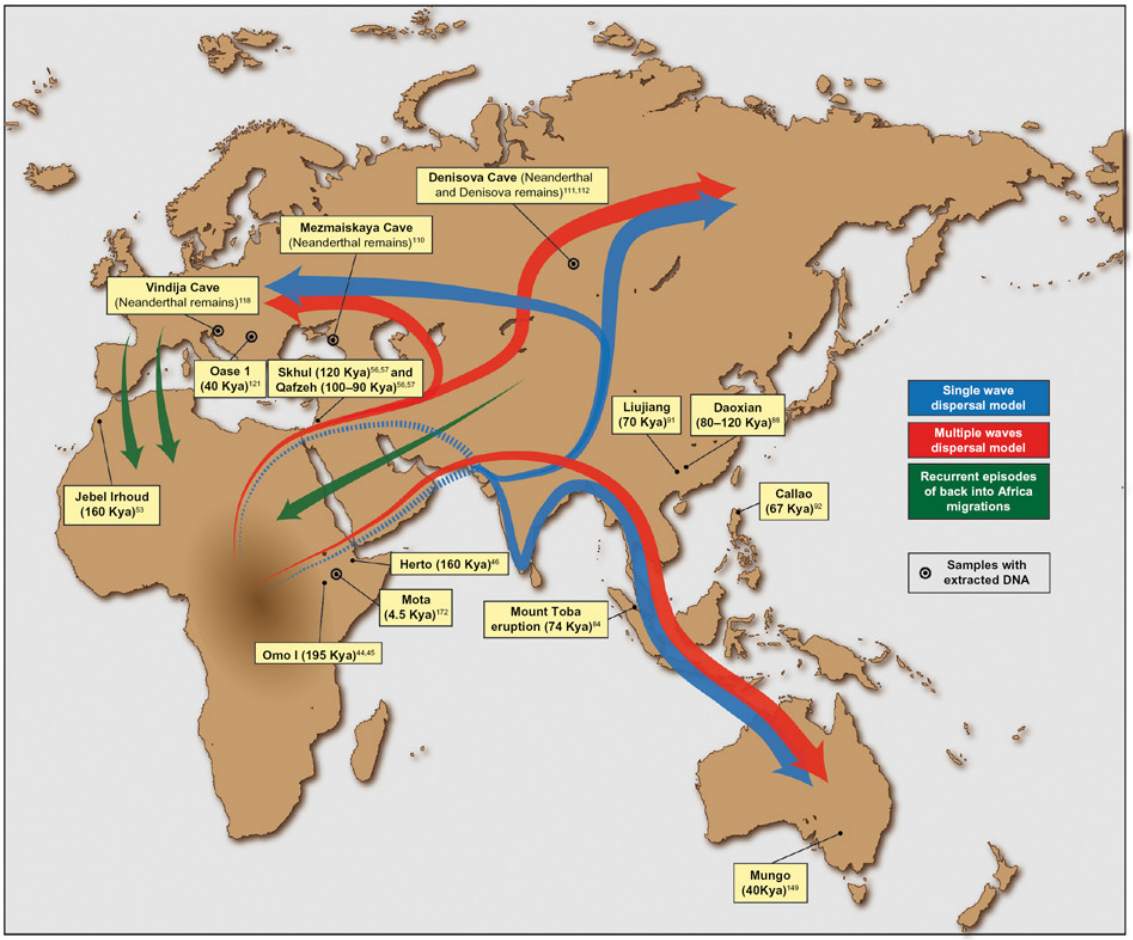

Figure 1: The map shows the presumed migration waves exiting Africa as well as a selection of the locations of the most important ancient human remains and archaeological sites. (López *et al.* 2015)

The habitable regions were mainly determined by climatic conditions (Banks *et al.* 2008). During the Last Glacial Maximum (LGM) at around 21 ka cal BP the ice sheet over Scandinavia and northern Europe reached its maximum volume. The climate in northern and western Europe was cold and generally arid. This forced humans to restrict

their range to southern European regions. Hence, there are only few archaeological sites and large gaps in the archaeological record for many regions from the time of the LGM (Banks *et al.* 2008). As shown in fig. 2, southeastern Europe however, was ice-free and hosted hunter-gatherer communities (Banks *et al.* 2008). Owing to these circumstances, there are continuous deposits in this region also from humans. This provides a unique opportunity to study the cultural evolution of AMH during that time.

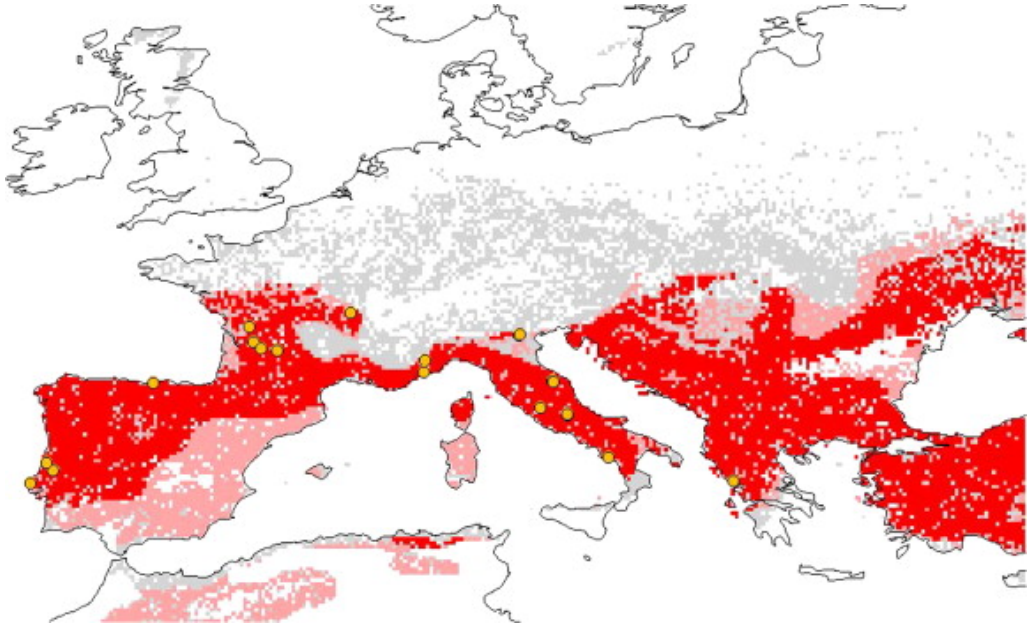

Figure 2: Prediction of human dispersal (eco-cultural niches) based on both Solutrean and Epigravettian sites dated to 21 ± 1 ka cal BP. Gray, pink and red designate the likelihood of an eco-cultural niche. Squares depicted in gray indicate that 1 - 5 of 10, pink 6 - 9 of 10 and red all 10 of 10 models predicted the presence of an eco-cultural niche. Archaeological site locations are indicated by yellow circles. (Banks *et al.* 2008)

In the Romanian Carpathians, glaciers were confined to elevations of 1600 m asl and above (Magyari *et al.* 2014) and many regions in today's Romania were thus ice-free during the LGM. Furthermore, Romania was located on the presumed route of AMH into Europe. Its key geographical position for the spread of AMH (Anghelinu *et al.* 2012) is also supported by findings of remains from AMH in a cave in southwestern Romania in 2002 (Trinkaus *et al.* 2003). They were dated to 34 - 36 ka uncal BP and therefore represent the oldest remains of AMH on European ground (Trinkaus *et al.* 2003). It is assumed that Romania's mountain valleys and basins were attractive to humans and animals alike as they provided shelter and refuge (Anghelinu *et al.* 2012, Schmidt *et al.* 2020). The Ceahlău area for example, is a hotspot for Upper Palaeolithic sites. Steguweit *et al.* 2009 suggest this might be owing to an abundance of fresh springs, generally relatively flat slopes and its role as transit area to neighbouring regions. Archaeological efforts in the Ceahlău basin began in the 1930s and were intensified in the 1950s before the realisation of a large dam construction project in the Bistriţa river (Steguweit *et al.* 2009, Anghelinu *et al.* 2018). The Bistriţa is one of eastern Romania's largest rivers. It flows from the Eastern Carpathians' northwest to their southeast, thereby providing relatively easy access through the mountain chain (Dumitraşcu & Vasile 2018).

Despite decades of scientific research, many facets of the regional cultural dynamics of the Upper Palaeolithic remain unclear. The unresolved questions include the detailed understanding of site formation as well as processes, cycles and palaeoecological contexts of human presence (Trandafir *et al.* 2015, Schmidt *et al.* 2020). This thesis aimed to contribute to the ongoing efforts and shed light on some of these uncertainties. The area of interest was a site in the Bistriţa valley, where layers displaying presumable combustion traces were discovered. To date, the genesis of these potential fire horizons, i.e. whether they originate from natural or anthropogenic fires, is unclear. The focus of the thesis was to gain insights on these combustion traces to get a better understanding of the palaeoenvironment. As the fires might directly relate to human occupation, differences between the fire horizons' composition could point to changes in usage. To a lesser extent, the palaeovegetation, which ultimately served as fuel for fires, was also investigated. Soil samples from the site in the Bistriţa valley were analyzed to investigate the following research questions:

1. Are the dark layers occurring at several depths of the profile traces of fire events?
2. If so, how highly energetic were the different fires?
3. How does the elemental composition of the fire horizons differ from that of the bulk material?
4. What type of vegetation was present at the time of the fires?

I hypothesized that the dark layers are indeed combustion traces (1) and that they exhibit a different chemical composition with increased contents of (black) carbon, nitrogen and other elements (2). Further, I hypothesized that the fires burned at low temperatures, i.e. were not very highly energetic (3). Lastly, I assume that a steppic vegetation consisting mainly of grass and only few trees was predominant (4). Answering the research questions required the application of several methods. The benzene polycarboxylic acid (BPCA) method was used to estimate the quantity and quality of black carbon in the soil. Lipid analyses helped to draw a picture of the palaeovegetation and was also insightful for the identification and characterization of fire horizons. Finally, X-Ray fluorescence (XRF) and elemental analysis were used to identify the chemical composition as well as the carbon and nitrogen contents of the samples.

2. Materials and methods

2.1. Study site

The Eastern Carpathian mountains in northeastern Romania are rich in loess deposits and contain numerous Upper Palaeolithic sites (Steguweit *et al.* 2009). The Bistriţa Valley, which is situated in the Ceahlău Basin, is part of the Eastern Carpathians. On the fluvial terraces of this valley several Upper Palaeolithic settlements exist, whereby the lower terrace and some of the sites were inundated after the construction of a dam in the middle of the 20th century (Nicolăescu-Plopşor et al. 1966 in Steguweit *et al.* 2009). One of the preserved settlements is the study site Bistricioara-Lutărie III (BL III) (fig. 3). It is situated on the right bank of the Bistrița river on a 16 to 18 m high, slightly inclined fluvial terrace (Trandafir *et al.* 2015). The silty to loamy colluvial and aeolian sediments covering the terrace are about 4.5 m thick (fig. 4, Schmidt *et al.* 2020).

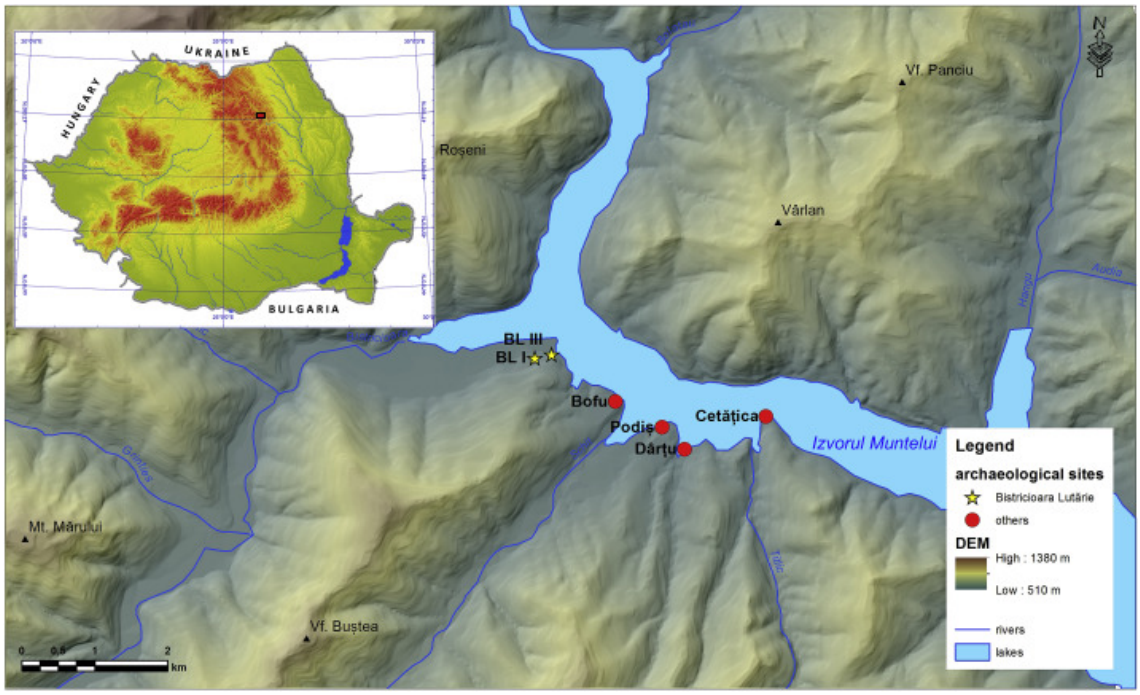

Figure 3: Relief map of the study area with the sample site BL III. The inset shows the location of the excavation site within the Carpathian Mountains in Romania. (Schmidt *et al.* 2020)

BL III lies in a mixed forest, which at the edge of the site is mainly dominated by coniferous trees. People from the region use the walls of the excavation profile to extract loam for their needs. The site was discovered in 2007 (Schmidt *et al.* 2020) and since then, two archaeological survey trenches have been investigated at this site. The first trench (S1) was excavated in 2013 (Trandafir *et al.* 2015) and the second (S2) in 2015, with results first published a couple of years later (Schmidt *et al.* 2020). Until 2018 six cultural layers had been discovered at BL III (fig. 4, table 1). They can be attributed to the Gravettian (28 - 25 ka cal BP), early Epigravettian (24 – 23 ka cal BP, around the LGM) and later Epigravettian (23 - 15 ka cal BP) (Schmidt *et al.* 2020). In the following, the profile at BL III will be briefly described based on the paper by Schmidt *et al.* 2020.

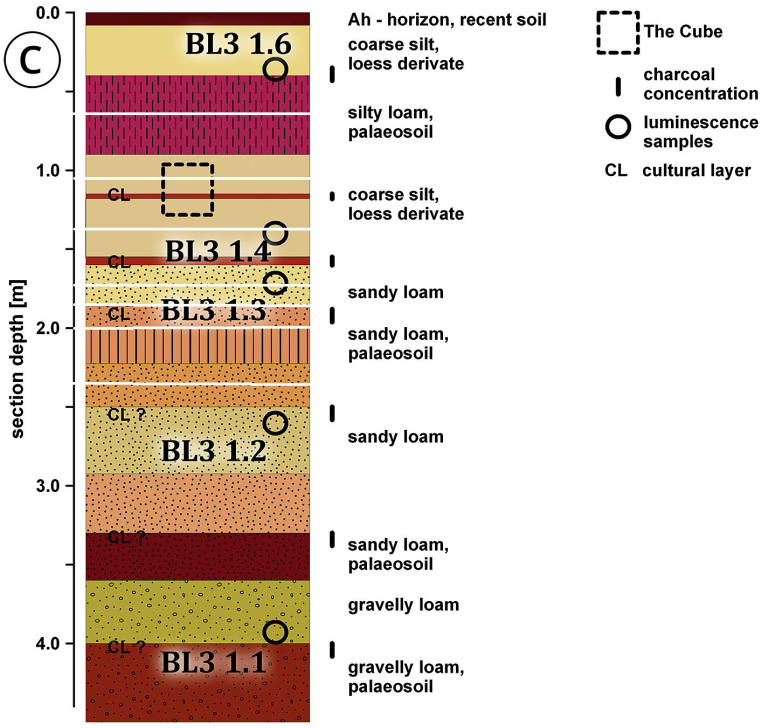

Figure 4: Sedimentary profile of BL III S1 (Trandafir *et al.* 2015). Horizontal, white lines represent the approximate depth of the sample blocks, which were taken from another section in the same wall.

At the top of the profile, loess derivates and reworked terrace sediments cover a palaesol horizon (cambisol). The sediment matrix in the uppermost 2 m consists mainly of silt, thin layers of sand and some single gravels. At around 1.7 – 1.8 m and 2.3 – 2.5 m depth a mottled, only initially developed pedo-horizon is embedded in light-colored silt containing also dark, presumably humic structures. Lacking signs of sediment relocation hint to pedogenesis and an aeolian origin of the silt in this area. While in-situ pedogenesis is prevalent at around 2 – 3 m, sediment relocation including soil material is dominant in the upper 3 m. At a depth of around 4 m a layer with combustion traces lies above partially laminated, red(dish) silt that covers a second layer of initial palaesols (polygenetic cambisols). The lamination could be attributed to weak relocation of the sediment within short distances or point to the repeated use of those spots as fireplaces. For a more in detail description see Schmidt *et al.* 2020.

In the course of excavations in the summer of 2018 (fig. B.23 in appendix B) seven blocks were taken from the profile at BL III. They were extracted from a third archaeological trench (S3), which is on the same excavation wall as S1 but due to clay mining, the wall has been changed, i.e. moved further backwards. The blocks lie at a depth of 0.65 m to 2.4 m, encompass a period of about 20 ka and contain different archaeological layers (table 1). Four blocks exhibit combustion traces (blocks 2, 3, 5, 6, fig. 5). Researchers have so far been unable to unravel the genesis of these presumable fire horizons.

Table 1: Overview of the sample blocks. The depths refer to the middle of the blocks. Information is based on Schmidt *et al.* 2020 and Trandafir *et al.* 2015 (marked with *). Age was determined by thermoluminescence on heated flints, optically stimulated luminescence on sedimentary quartz and radiocarbon dating of charcoal.

block	depth [cm]	cultural layer	pedological horizon	age [ka cal BP]
7	64	-	gelistagnic cambisol	15.3 ± 1.0 (at 72 cm)
6	105	Early Epigravettian	-	20.5 ± 2.9 (at 108 cm) *
5	135	Early Epigravettian	-	26.5 ± 2.6 (at 142 cm) *
4	170	Gravettian	-	29.3 ± 2.9 (at 172 cm) *
3	185	Gravettian	-	27.346–27.773 (at 186 cm)
2	200	Gravettian	-	27.873–28.515 (at 196 cm) *
1	237	Gravettian	polygenetic (forest-?)cambisol	35.180–36.384 (at 237 cm)

(a) (b)

Figure 5: Fire traces in the profile at BL III. Block 2 is shown in (a), blocks 5 and 6 are shown in (b). (pictures: U. Hambach)

2.2. Sample preparation

All blocks were characterized by very fine, silt dominated material, which included glimmer (presumably Muskovit). Some isolated pebbles could be found but this solid fraction was negligible compared to the bulk material.

In every block, the outer 2 to 5 mm of all sides were cut off using a ceramic knife. This step ensured that no lipids that are naturally present on the human skin and might have contaminated the surface during sampling would distort the results of the lipid analysis. As this was not possible for the back sides due to their uneven surface structure, they were thoroughly cleaned using a brush. Samples were then taken by visually identifying changes in the color that were assumed to be meaningful. A portable X-Ray fluorescence device did not prove to be useful in that context as the measured elemental contents hardly varied. The samples were assigned a lab code, whereby the sample number increased with depth. Samples were then homogenized with pestle and mortar, sieved through a 2 mm sieve to

separate roots and pebbles, and milled using a horizontal ball mill (Retsch MM 400). In the next few paragraphs all blocks will be briefly described. A list with all the samples can be found in appendix A.

2.2.1. Block 1

Block 1 was located at a depth of 237 cm. The upper part of the front side displayed a darker, brown/reddish color (see fig. 6b), which might be attributed to a higher iron content. This could also be observed in the lower left when looking at the block from the top. Additionally, on the top side there was a grey, round spot with a diameter of 9 mm (see fig. 6a). Throughout the block some isolated black spots - presumably rich in carbon - could be found, especially at the top side. There were also some larger (>2 mm) biopores. One in the front side was filled with a 2.5 cm long root. As shown in fig. 6b four samples were taken from this block. The first one contained the brown-red area in the upper part, the second was taken straight below. The third was taken below the middle and above the fourth sample, which included the part at the bottom with a slightly lighter color. Between the second and the third samples however, there was no obvious visual difference.

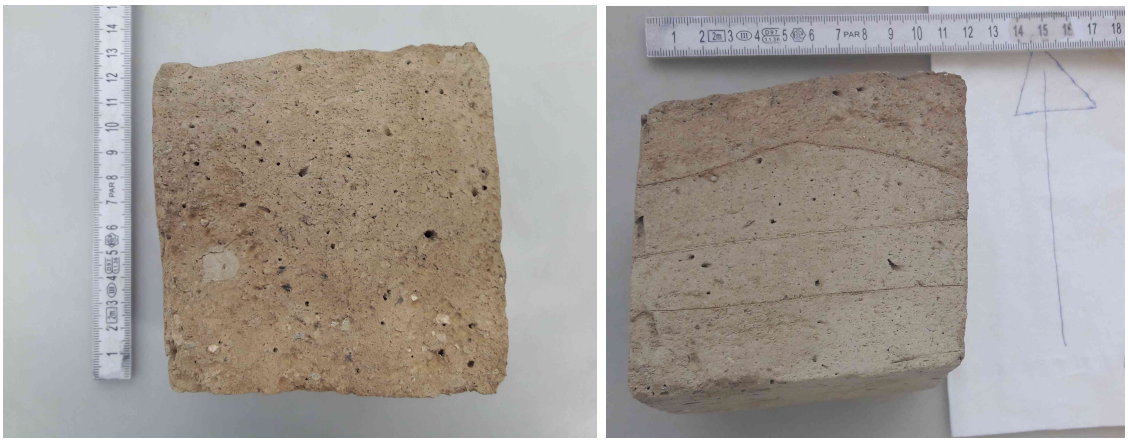

(a) (b)

Figure 6: The top of block 1 after abrading the outer layer is seen in (a). The lines scratched into the front side (b) mark where the samples were taken. Orientation is the same as in the field. Note that the lighting conditions influence the color of the blocks in the pictures.

2.2.2. Block 2

Block 2 was taken at a depth of 200 cm. It was characterized by a dark layer visible on the left, front and right side (see fig. 7). Potentially, the dark layer could be the result of fire event(s). According to Ulrich Hambach (personal communication) the dark horizon has a large horizontal expansion covering at least several hundred square meters. However, apart from the presumable combustion traces there are no specific characteristics and it is completely free from macroscopic remains of human activity (e.g. artifacts). Sedimentological features indicate that thawed millimeter thin layers of sediment have been washed away (personal communication, U. Hambach). In the block, the dark horizon is accompanied above and below by an area with a brown-orange, even slightly purplish

color. This coloration could also be observed at the right corner of the top side, in the top left corner of the back side and spanning as a band above the dark layer both on the left and right side of the block. Traces of roots were found in the lower third of the front side as well as on the back side. At the top middle of the right side there was a longish hole (see fig. 7b).

From this block, five samples were taken: The first was clearly above the dark layer and the brown-orange band. One was taken within the band but above the dark layer, one in the dark layer (see the two areas separated by the scratched line in fig. 7d), the next slightly below and one clearly below the layer and the band.

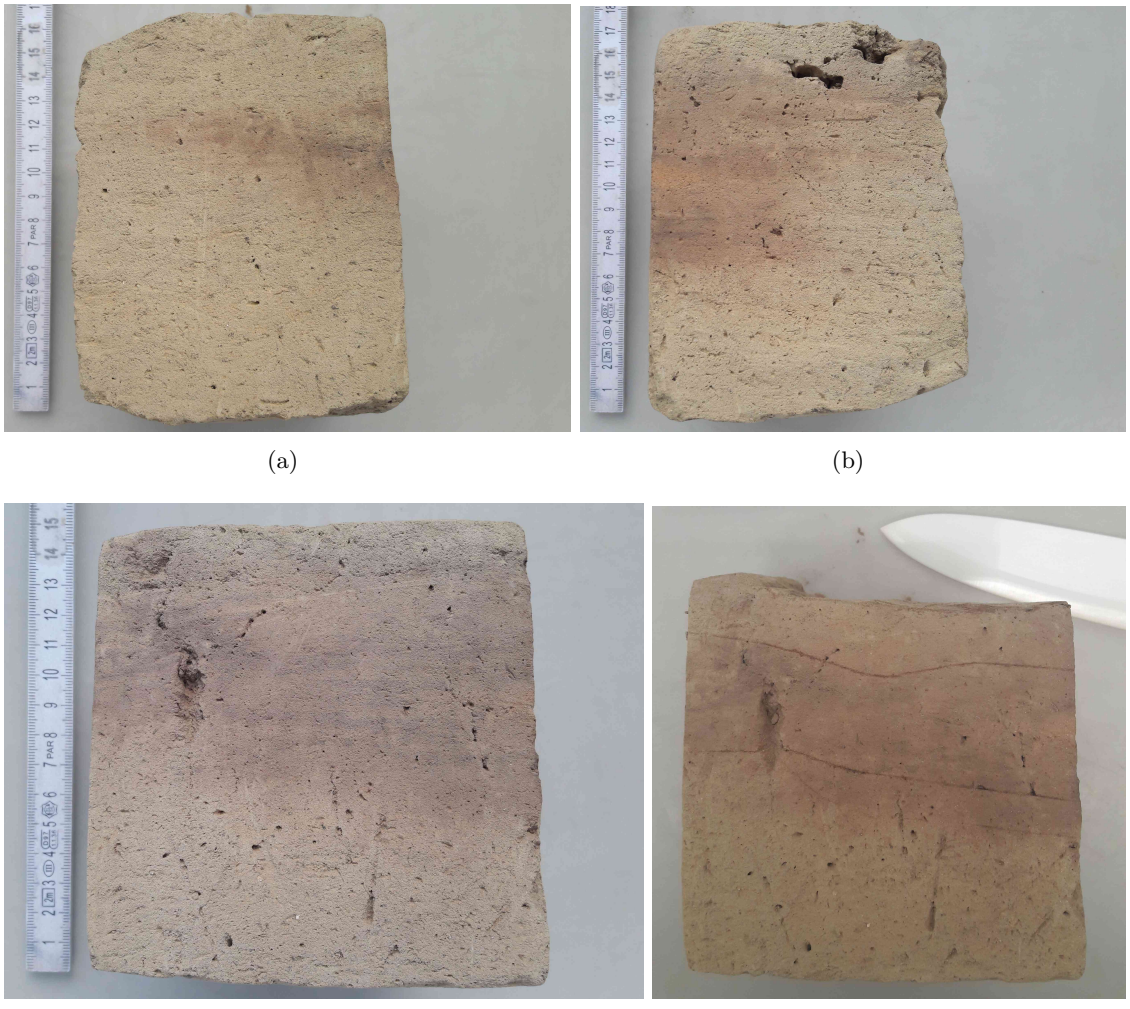

(a) (b)

(c) (d)

Figure 7: The presumable fire horizon spanning through the left (a), right (b) and front (c) side of block 2. Picture (d) shows the sampling locations: The scratched lines in the upper part mark the areas from each of which one sample was taken. Two more were taken in the lower part, while one in the upper right corner had already been taken. Different colors of the block in the pictures are due to lighting.

2.2.3. Block 3

Block 3 was taken at a depth of 185 cm. The most apparent feature were some soft, brown pieces, most likely wood, especially in the front and right side (see fig. 8a).

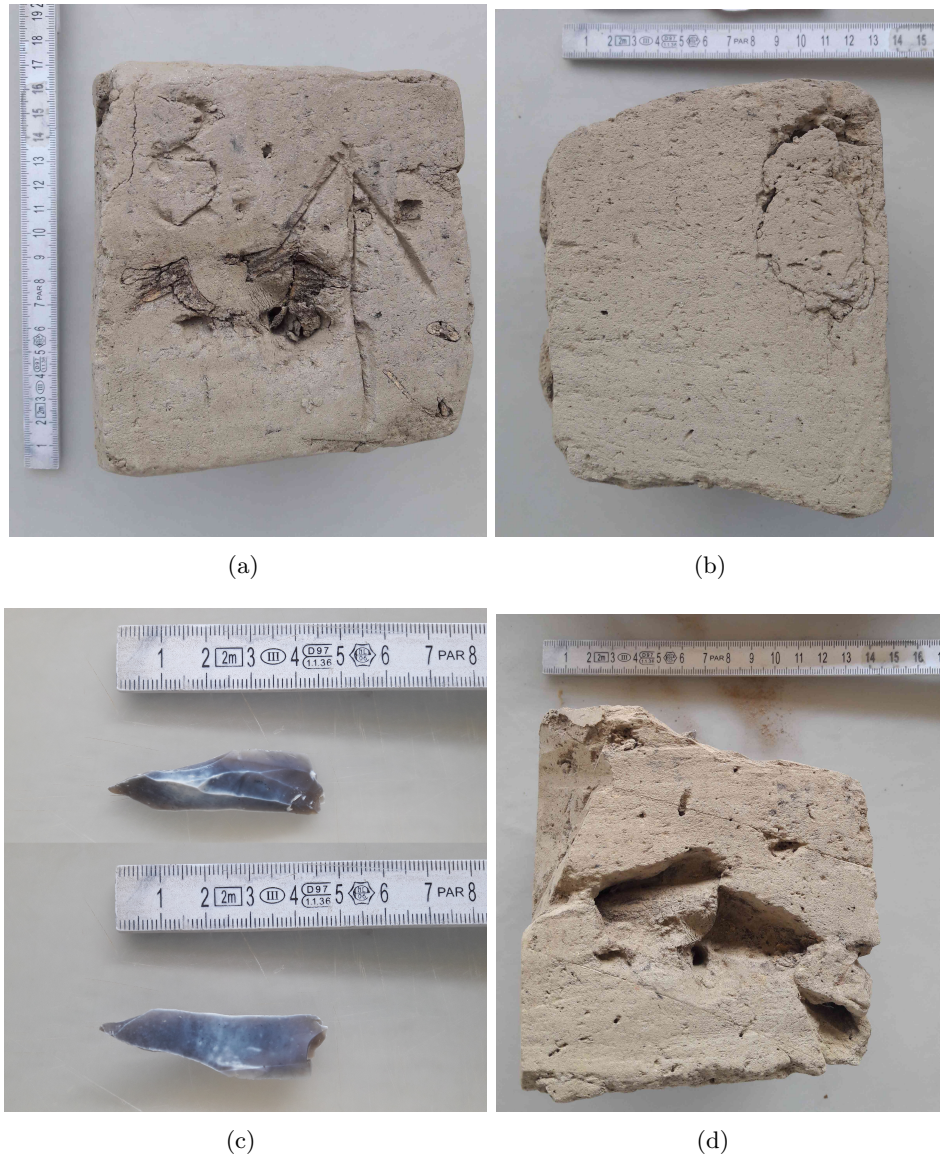

(a) (b)

(c) (d)

Figure 8: Block 3 shown from the front (a) before abrading and recovering the wood. Picture (b) shows the fragment in the top of the block's left side. The front and back side of the artifact that was found can be seen in (c). In picture (d) the sampling locations of three samples are marked by the scratched lines. Two samples on the left side as well as on the top right had already been taken.

The wood was collected but excluded from all analysis except X-Ray fluorescence. After the wood had been removed, it became apparent that the upper area had a noticeably darker color than the lower part of the block. On the left side there was a loose fragment (ca. 25 x 53 mm, see fig. 8b), which fell off during the preparation of the block.

Throughout the block several small fragments of a hard, white material (probably some kind of stone or bones) and a larger artifact with a dark, blueish color (likely a blade, see fig. 8c) were recovered. They were given a lab code but were not analyzed. In several locations of the block some very small red spots were visible. They too were collected as an individual sample but due to the small sample amount could not be analyzed with the exception of elemental analysis.

Apart from the wood, the red spots and the artifacts five samples were taken from this block. The first one was the fragment that fell off from the top left corner when viewed from the front. A second sample was taken in the top right corner above the darker area while another one was taken from the darker layer itself. Material from the areas where wood was recovered, was collected as a fourth sample. The last sample was taken at the bottom left that was completely wood-free and had a lighter color.

2.2.4. Block 4

Block 4 was retrieved at a depth of 170 cm. On all sides except the top, traces of carbon accumulation were visible as dark spots. At the bottom edge of the right side there was a charcoal piece (fig. 9a), which was retrieved for analysis. As it contained only little material, lipid analysis and X-ray fluorescence could not be performed on this sample.

Traces of former roots could be found on the front and back side. On the top and left side, a marbling with light and rust-brown colors was apparent (fig. 9b). The first sample was thus taken in the top left corner of the front side, which was characterized by a lighter color. Another sample was taken diagonally below and then again below that one (fig. 9c). The last samples were taken from the part below the middle and the bottom. All the samples were separated along contours, where slight changes in color occurred.

(a) (b)

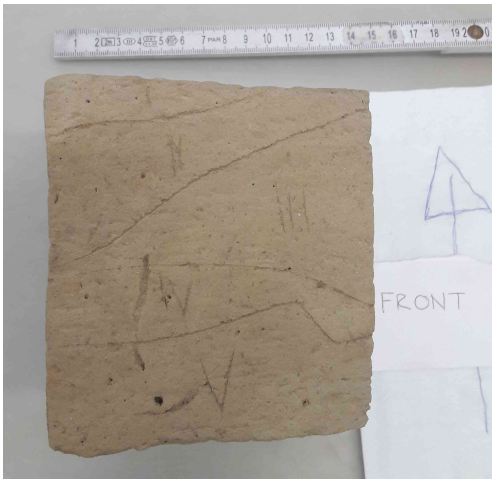

(c)

Figure 9: In (a) the right side of block 4 before abrading is shown. The charcoal piece at the bottom edge was recovered for analysis. On the top side (b) a variation in color with some lighter and some rusty-colored areas is visible. Samples were taken at the locations marked in (c).

2.2.5. Block 5

Block 5 was taken at a depth of 135 cm. The most striking characteristic was a dark layer that is believed to be a fire horizon. These presumable combustion traces could be observed at the left, right, front and back side (fig. 10). Within the layer some small charcoal pieces could be found. Apart from that however, there were not many signs of carbon accumulations (i.e. dark spots) outside this layer. One sample each was taken both clearly and slightly above, and clearly and slightly below as well as inside the presumed fire horizon.

(a) (b)

(c) (d)

Figure 10: The presumable fire horizon can be observed in the left (a), the right (b) and the front (c) side of block 5. The oddly colored residue in the shape of a snail is shown in (d).

On the top and right side there was a rounded coloring (fig. 10b & d) with a dark brown lining on one side and gradually lighter colors towards the other side. Its shape reminds of a snail, which might have decomposed at this location. The shape was cut out and given a sample code for analysis.

The block also contained some fine roots on the right, left and back side as well as some traces of former roots on the back side. The material around the roots was recovered and analyzed as a rhizosphere sample.

2.2.6. Block 6

Block 6 was taken at a depth of 105 cm. The block contained a dark horizon, presumably caused by fire. It was visible as a dark band that extended around the whole block (fig. 11a - d). One sample each was taken both clearly and slightly above, and clearly and slightly below as well as inside the presumed fire horizon on the left side of the block.

Another striking feature was a whitish orange marbling mainly at the front and top side, but also, although less pronounced, at the left, right and the bottom (fig. 11a - c, e & f) side. On the front side there were also some gray areas (fig. 11c) which could be remains of former burrows. They turned out to be connected and were separated as a sample.

In the right, upper part of the back side, a hard, flat piece was sticking out (fig. 11d). It was separated but not analyzed. Whether it is a regular stone or an artifact, e.g. a tool, is unclear. Some single, fine roots could be found on all sides. As in block 5, the material around the roots was collected and analyzed as a rhizosphere sample.

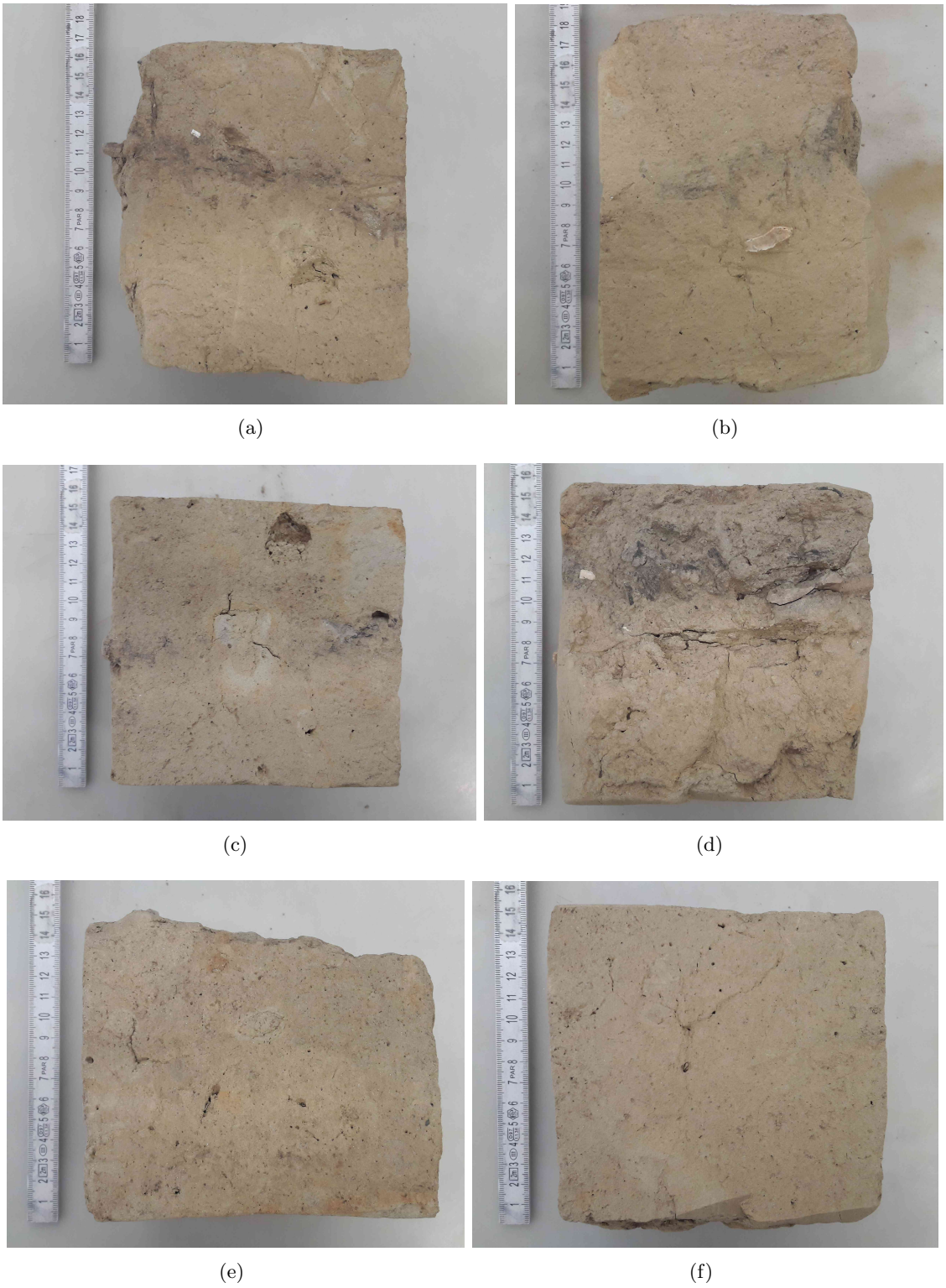

(a) (b) (c) (d) (e) (f)

Figure 11: The presumable fire horizon is visible in the left (a), the right (b), the front (c) and the back (d) side of block 6. Pictures (e) and (f) show the top and bottom side respectively, where the marbling occurring at several sides of the block can be seen.

2.2.7. Block 7

Block 7 was the uppermost block, sampled at a depth of 64 cm. The left, bottom and to a lesser degree the top side displayed a whitish and orange marbling (fig. 12). Additionally, some singular orange areas in the front and back could be observed.

(a) (b)

(c) (d)

Figure 12: Picture (a) shows the right side of block 7, where a block fell off along break lines. The left (b) and bottom (c) side display a whitish-orange marbling. In the front side (d) a breaking line in the top right and an orange-colored line in the bottom left are visible.

On several sides some fine roots could be found. Again, the material around the roots was collected as a rhizosphere sample. On the front, bottom and top side some dark spots, most likely carbon accumulations, could be observed.

In total, four samples were taken: They were taken along breaking lines on the front side (fig. 12d), starting from the upper right-hand corner and then diagonally towards the lower left. The last sample was taken along the orange line in the lower left corner.

2.3. Sample classification

Samples were summarized in the following sample groups: presumable fire horizons (n = 4), samples directly above fire horizons (n = 4), samples directly below fire horizons (n = 4), rhizosphere (n = 3) and bulk samples (n = 23 - 25 depending on the analysis). The roots that were separated by sieving got destroyed during milling and could unfortunately not be analyzed.

As described above, the presumable fire horizons were located in blocks 2, 3, 5 and 6. For ease of reference these individual horizons will be referred to as fire 2, fire 3, fire 5 and fire 6 respectively. Also, to improve readability the "presumed" will be omitted when talking about the presumable fire horizons.

The charcoal sample from block 4 was excluded from all groups as it is neither a fire horizon nor a regular bulk sample. When included in the bulk samples it acts as an outlier distorting the mean values and increasing the standard error of the mean. Nevertheless, the sample's results are useful to compare with those of the fire horizons because it has also been exposed to fire.

2.4. Carbon and nitrogen contents

The carbon (C) and nitrogen (N) contents were measured with an elemental analyzer (Thermo Fisher Flash HT) coupled via ConFlo IV to Delta V Plus isotope ratio mass spectrometer to derive the isotopic signature. Based on the expected carbon concentrations, 10 to 15 mg of milled sample material was filled into tin capsules for analysis. By adding hydrochloric acid during the preparation of the blocks, it had previously been determined that no carbonate was present in the samples. Accordingly, the measured carbon contents correspond to the total organic carbon (TOC) content. Carbon isotopic values (‰) were calculated as follows:

$$\delta^{13}C = \left(\frac{{}^{13}C/{}^{12}C_{\text{sample}}}{{}^{13}C/{}^{12}C_{\text{standard}}} - 1\right) \cdot 10^3 \tag{1}$$

where

$${}^{13}C/{}^{12}C_{\text{standard}} = \quad 0.0112372 \text{ (Vienna Pee Dee Belemnite (V-PDB) standard)}$$

2.5. X-Ray fluorescence

To investigate the atomic elemental composition of the samples X-Ray fluorescence (XRF) analysis was performed using Spectro Xepos, AMETEK. The measured element contents were converted into their oxide form by applying conversion factors based on molar weight. They were then standardized with titanium oxide. This procedure allowed to eliminate measurement inaccuracies.

2.6. Lipid analyses

Extraction of free extractable lipids and their separation into the different fractions were performed according to Wiesenberg & Gocke 2015. For the Soxhlet extraction an aliquot of each sample (∼15 g to 20 g) was extracted during at least 24 h (up to 45 h) using a mixture of dichlormethane (DCM)/methanol (93:7, v:v). As the amount of free fatty acids in the sample was expected to be minor, the obtained total lipid extracts (TLE) were regarded as the neutral fraction. After the solvent had completely evaporated, the neutral fraction was split into aliphatic and aromatic hydrocarbons as well as low polarity hetero compounds. To do so, the neutral fractions were dissolved in solvent mixtures of hexane, hexane/DCM (1:1, v:v) and DCM/methanol (93:7, v:v) and put on columns filled with activated silica gel (100 Å, Supelco) (Gocke *et al.* 2013). Before measuring the aliphatic hydrocarbons 40 µl deuteriated standard ($D_{50}C_{24}$ *n*-alkane, concentration = 0.10456) was added for quantification. Aliphatic hydrocarbons were then measured with a gas chromatograph furnished with a flame ionisation detector (GC-FID, Agilent 7890B). Preliminary GC-FID measurements revealed low *n*-alkane contents. To improve the measurement accuracy the aliphatic hydrocarbon fractions were therefore concentrated by further reducing the amount of solvent and transferring them to glass inlets that were put in clear autosampler vials. 1 µl of sample solution was injected via multi-mode inlet at 70 °C. After 4 min of isothermal conditions, the temperature was raised at a rate of 5 °C min^{-1} to 320 °C. This temperature was then held for 20 min.

Initial test measurement of polycyclic aromatic hydrocarbons (PAH) using selected ion monitoring (SIM) with GC-MS for the presumable fire horizons revealed very low concentrations. It was hence decided not to pursue this analysis further.

2.7. Lipid molecular proxies

(*n*-alkanes) are important constituents of epicuticular leaf waxes. They can be preserved in soils and sediments over geological time-scales, which makes them valuable for palaeoclimatic, palaeovegetational and palaeoenvironmental research (Bush & McInerney 2013, Schäfer *et al.* 2016, Obreht *et al.* 2019). Their distribution as well as the range and variation of *n*-alkane chain lengths have been utilized as a molecular proxy for almost a century (Bush & McInerney 2013). They are also frequently applied in chemotaxonomic studies to differentiate plants (Eglinton *et al.* 1962, Jansen & Wiesenberg 2017)

Average chain length

One of the most common methods to characterize *n*-alkane distributions is the average chain length (ACL). *n*-alkanes with long chains (≥ 25 C atoms) are indicative of higher plant epicuticular waxes, while short chain *n*-alkanes point to organic matter (OM) derived from degradation or microbial and/or aquatic origin (Eglinton *et al.* 1962; Kolattukudy *et al.* 1976; Obreht *et al.* 2019). It has been documented that, owing to the cracking of C bonds, ACL also decreases during charring at high temperatures, i.e. thermal degradation (Wiesenberg *et al.* 2009).

ACL was calculated as follows (Bush & McInerney 2013):

$$ACL = \frac{\sum C_n \cdot n}{\sum C_n} \tag{2}$$

where

C_n abundance of each n-alkane with n C atoms
n number of C atoms in the range of 16 - 33

Carbon preference index

The carbon preference index (CPI) describes the relative abundance of chain lengths with an odd number of carbon atoms compared to those with an even number of carbon atoms. Fresh leaf biomass of higher plants usually displays a strong predominance of odd carbon-number alkanes (Eglinton *et al.* 1962). A decrease of this odd predominance is often the result of OM degradation or microorganism-derived OM and leads to CPI values <10 (Cranwell 1981). In turn, values >10 are indicative for fresh aboveground plant biomass (Cranwell 1981). CPI can therefore serve as an indicator of alteration intensity of the odd over even predominance in alkane distribution (Buggle *et al.* 2010). It was derived with the following equation (Gocke *et al.* 2013):

$$CPI = (\frac{\sum n - C_{25-33odd}}{\sum n - C_{24-32even}} + \frac{\sum n - C_{25-33odd}}{\sum n - C_{26-34even}})/2 \tag{3}$$

Short-chain n-alkanes

Researchers have found that thermal degradation of OM alters lipid distribution patterns in a way that can be distinguished from those stemming from microbial degradation (Eckmeier & Wiesenberg 2009). The observed lipid pattern changes depend on the charring temperature but not on the charring duration and only little on the fuel source (Wolf *et al.* 2013 Wiesenberg *et al.* 2009). At high temperatures (500 °C) an increase in even numbered, short chain n-alkanes with a maximum at C_{16} and/or C_{18} has been reported (Eckmeier & Wiesenberg 2009, Wiesenberg *et al.* 2009). This enrichment in even short-chain lengths is also reflected in the increase of CPI_{short}:

$$CPI_{short} = (\frac{n - C_{16} + n - C_{18}}{n - C_{15} + n - C_{17}} + \frac{n - C_{16} + n - C_{18}}{n - C_{17} + n - C_{19}})/2 \tag{4}$$

Ratio of C_{27}/C_{31} alkanes

Grasses and herbs are commonly dominated by C_{31} or C_{33} alkanes, while trees are often rich in C_{27} alkanes and C_{29} alkanes (Schwark *et al.* 2002, Lei *et al.* 2010, Obreht *et al.* 2019, Gocke *et al.* 2014). Ratios such as C_{27}/C_{31} (e.g. Zech *et al.* 2009, Gocke *et al.* 2013) or $(C_{27} + C_{29})/C_{31}$ (e.g. Lei *et al.* 2010) have therefore been widely used for distinguishing between trees and shrubs versus grasses and herbs as the dominant source of OM (Schwark *et al.* 2002). It has also been shown that due to OM degradation these ratios decrease during decomposition and the formation of soil OM (Zech *et al.* 2009, Obreht *et al.* 2019).

2.8. Black carbon analyses using the BPCA method

The combustion of OM under local or temporal oxygen limitations produces carbon rich, organic residues (Bird & Ascough 2012, Wiedemeier *et al.* 2016). These residues are high in black carbon (BC), also called pyrogenic carbon, which consists of condensed aromatic rings. They are very persistent in the environment and relatively stable against microbial decomposition (Kuzyakov *et al.* 2009). BC can serve as a tracer for both natural and anthropogenic fire history (Glaser *et al.* 1998, Schmidt & Noack 2000). As BC is not directly accessible with chromatographic means its highly aromatic core first needs to be broken down (Wiedemeier *et al.* 2016). This is achieved by nitric acid oxidation under high temperature and pressure, which leads to the formation of benzene polycarboxylic acids (BPCA) (Wiedemeier *et al.* 2016).

To quantify and characterize the BC present in the samples, the protocol of Wiedemeier *et al.* 2016 was applied. For BPCA assessment about 500 mg to 1000 mg of milled sample material and ∼250 mg of an external standard (Chernozem) was weighed into quartz tubes. For half of the samples a duplicate was prepared. The amount of sample material used, was determined based on the measured TOC content. The goal was to ensure that each sample aliquot contained between 5 and 10 mg of C. The aliquots were then treated with 2 ml of 65 % HNO_3 for 8 h 10 min at 170 °C using sealed pressure chambers. The samples were diluted with Millipore water and filtered through disposable glass fiber filters. The resulting samples were put on columns containing conditioned cation exchange resin and then freeze-dried (Christ Alpha 1-2). Next, the samples were dissolved in 3 ml of methanol/water (1:1, v:v). An aliquot of 1.5 ml of redissolved sample was eluted over a conditioned C18 solid phase extraction cartridge (Supelco Discovery DSC-18, 3 ml tubes) and then dried (eppendorf Concentrator plus). The dry residues were redissolved in 1 ml water and transferred to autosampler vials. BPCA separation was done using an Agilent 1290 Infinity HPLC system with a binary pump and Agilent Poroshell 120 SB-C18 column (100 mm × 4.6 mm). A UV-diode array detector was used for peak identification and quantification (absorption at 240 nm). A calibration curve was generated with standard solutions of BPCA.

After all HPLC measurements had been done, it was found that the cation exchange resin needed to be replaced. This indicated that the measured BPCA contents were most likely too low. It was hence decided to repeat some samples (labcodes 213B19DB3, 213B19DB6, 213B19DB11, 213B19DB14, 213B19DB22, 213B19DB31, 213B19DB40) including duplicates for half of them. For each sample, all measurement results were checked for inconsistencies. If a result seemed very odd, e.g. due to a mistake during the execution of the BPCA protocol, it was excluded. The average of all meaningful results of a sample was then calculated and used for further analysis. However, the values generally looked plausible with standard deviations lower than 30 %.

The total amount of carboxylic acids after oxidation represents a marker for the original amount of polyaromatic carbon (Glaser *et al.* 1998). Therefore, the aromaticity was determined as the total amount of BPCA per organic carbon (BPCA-C g kg^{-1} TOC) (Budai *et al.* 2017, Wiedemeier *et al.* 2013). The proportion of the individual BPCAs mirrors the size of the original polycyclic structure (Wiedemeier *et al.* 2016). As B6CA can only originate from the center of the BC molecule, high proportions of B6CA imply a higher degree of aromatic condensation of a sample and - linked to that - higher pyrolysis temperatures (Schneider *et al.* 2010, Wiedemeier *et al.* 2016). The degree of aromatic condensation was described as the ratio of products with 5 and 6 carboxyl acidic groups, i.e. B5CA/B6CA (Wolf *et al.* 2013).

2.9. Statistical analyses

For analyzing and plotting the data, Microsoft Excel (Version 2001) and MATLAB (R2019b Update 3) were used. Means and standard errors of the mean were calculated for sample types, blocks and the whole sample set. All data was tested for normal distribution with the Kolmogorov-Smirnov-Test on standardized data and by generating normal plots. If the data was normally distributed, one-way ANOVA with $\alpha = 0.05$ was performed to test for significant differences between blocks and sample types. As a single outlier can make an otherwise significant result insignificant, data was first checked for outliers. As a consequence thereof, the charcoal piece (labcode 213B19DB21) was not included in ANOVA. Also, fire horizons were excluded when investigating significant differences between blocks since they might mask differences between blocks by distorting the mean values of the blocks containing a fire horizon. ANOVA was followed by post-hoc F-test. If the condition of normal distribution was not met, a Kruskal-Wallis Test ($\alpha = 0.05$), followed by post-hoc Chi-squared test was performed instead of one-way ANOVA.

3. Results

All data can be found in appendix A.

3.1. Elemental composition

Carbon concentrations ranged from 1.9 mg g^{-1} sample weight in the bulk sample clearly below the fire horizon in block 5 to 11 mg g^{-1} in the charcoal sample. The average concentration was 3.4 ± 0.3 mg g^{-1}. The relatively high standard error can be explained by the high C content of the charcoal sample. With the exception of fire horizons and the charcoal sample, C concentrations were quite similar within individual blocks. Comparison of blocks revealed significantly lower C yields in block 5 than blocks 3 ($p = 0.04$) and 6 ($p = 0.01$). The high average C contents in blocks 3 and 6 were the result of some samples with remarkably high concentrations that elevated the average C contents of those blocks. The sample above the fire horizon in block 3 for example, exhibited 9.5 mg C g^{-1} sample weight, which is almost three times larger than the overall average C content. The high variability within those blocks is also reflected in high standard errors. For an illustration of the average C and N contents in the different blocks consider figs. C.24 and C.25 in appendix C.

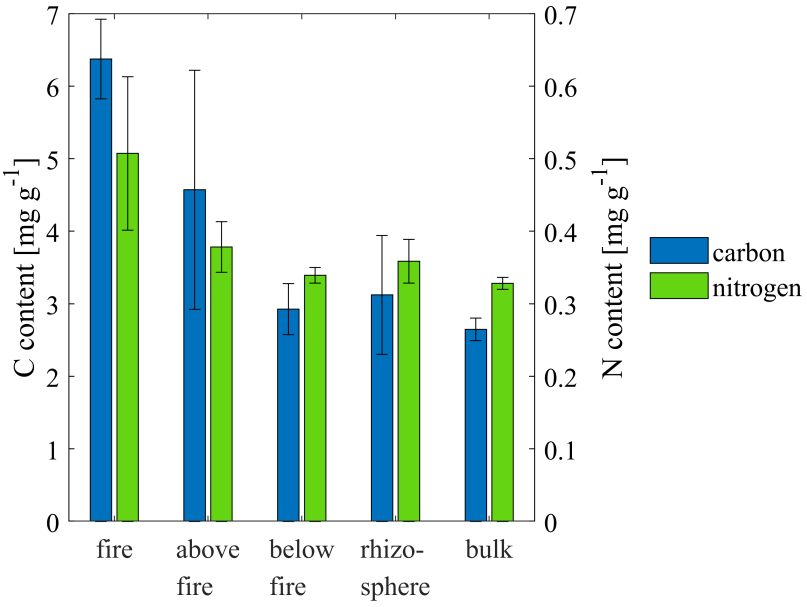

Figure 13: Average C and N contents of the sample groups. Low N concentrations are apparent for all sample types. Nevertheless, the higher concentrations for the fire horizons become apparent. The pattern was also observed for C concentrations. Bars represent the standard error of the mean. As discussed in the text, very large errors for C in the group "above fire horizon" are the result of the extremely high concentration in the sample in block 3 and the comparatively low concentration in the one from block 5.

The range of nitrogen contents spanned from 0.27 to 0.82 mg g^{-1} and reached an average of 0.35 ± 0.01 mg g^{-1}. Even if only just, there was no significant difference ($p = 0.053$) for the N contents between blocks. However, for both N and C contents, the difference between sample groups reached significance ($p = 0.002$ and $p = 0.01$, respectively).

Samples in fire horizons (6.4 ± 0.5 mg g^{-1}) contained significantly more C than bulk samples (2.6 ± 0.2 mg g^{-1}). Samples above fire horizons exhibited a C concentration of 4.6 ± 1.6 mg g^{-1}, followed by rhizosphere (3.1 ± 0.8 mg g^{-1}) and samples below fire (2.9 ± 0.4 mg g^{-1}). This is also illustrated in fig. 13.

N concentrations displayed the same pattern with highest amounts for fire (0.51 ± 0.1 mg g^{-1}), samples above fire (0.38 ± 0.04 mg g^{-1}), rhizosphere (0.36 ± 0.03 mg g^{-1}) and finally samples below fire horizons (0.34 ± 0.01 mg g^{-1}) and bulk (0.33 ± 0.01 mg g^{-1}). The relatively high standard error for the fire samples can be attributed to the high N concentration (almost double of the overall average) in the fire horizon in block 2.

The C/N ratio did not differ significantly between sample types ($p = 0.14$) but between blocks ($p = 0.0002$). As apparent in fig. 14a, this is however only due to a very high average C/N ratio in block 3 at a depth of 185 cm. This block contained many woody residues. As wood usually exhibits a very high C/N ratio (Clausen 1996), this might explain the higher values in block 3. However, the high standard error of the mean reflects that within this block, the values for the C/N ratio varied quite substantially. They ranged from 10 (sample taken from the block that was falling out) to 24 (sample above the fire horizon). All in all, it seems evident that a depth dependent trend is lacking. The C/N ratio does therefore not imply a more advanced degradation towards the bottom of the profile.

ANOVA revealed the same pattern for the carbon isotopic signature (δ^{13}C), with block 3 displaying a different δ^{13}C signature than all other blocks except block 1 at the bottom (fig. 14b). Additionally, block 7 had significantly lower values than blocks 1, 3 and 6. Over the whole sample set, values ranged from -26.3 to -23.6 ‰, with an average of -25.3 ± 0.1 ‰. ANOVA and F-test showed that the isotopic signature of fire horizons (-24.2 ± 0.2 ‰) differed significantly from all other sample types ($p = 0.01$). Isotopic values for samples above and below fire horizons were virtually the same (-25.1 ± 0.3 and -25.2 ± 0.4 ‰, respectively). Values for bulk samples (-25.6 ± 0.1 ‰) and rhizosphere samples (-25.7 ± 0.3 ‰) were also very similar. For an illustrative comparison of the isotopic signatures and the C/N ratio between groups see fig. C.26 in appendix C.

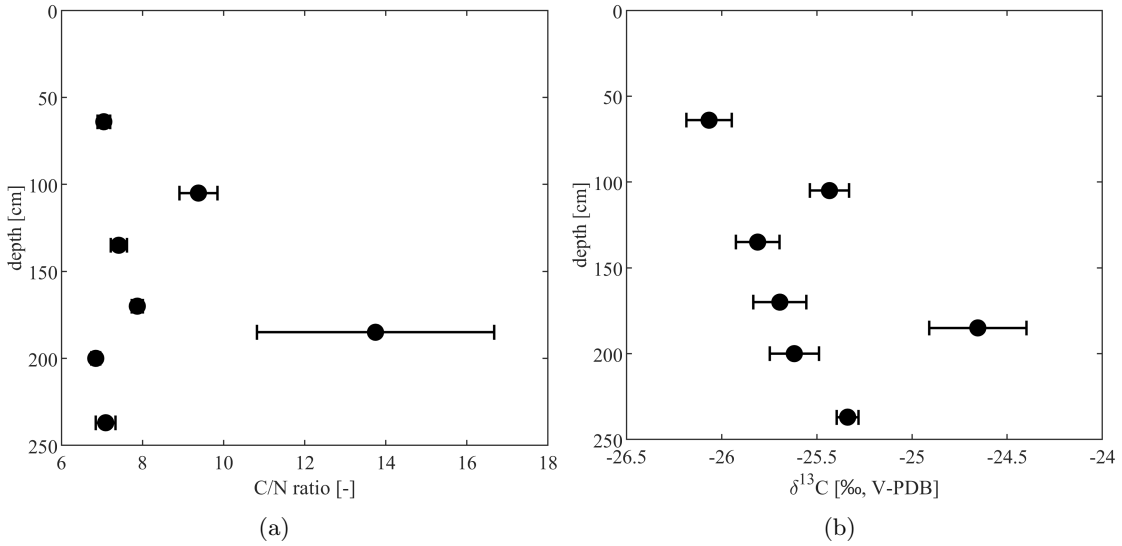

Figure 14: The mean and standard error of the mean of the C/N ratio (a) and of the isotopic signature, i.e. δ^{13}C, V-PDB (b) for the seven blocks.

Atomic elemental abundance as revealed by XRF analysis showed that the differences in the chemical composition were only very small. This was true with regards to sample type as well as depth. When comparing sample groups, differences in elemental abundance were only statistically significant for a handful of elements: Cu with $p = 0.002$, Cr with $p = 0.01$, Si with $p = 0.01$, K with $p = 0.04$ and V with $p = 0.05$. The differences are summarized in table 2. While Kruskal-Wallis test resulted in no significant differences between groups for germanium (Ge), Chi-squared test still revealed a difference ($p = 0.02$) between samples in fire horizons and bulk samples. The opposite was true for potassium, where p was $<\alpha$ but Chi-squared test did not detect significant differences between sample groups.

The differences in the abundance of CuO/TiO_2 seemed to be the most interesting. While CuO/TiO_2 did not differ between blocks (see also fig. C.27), fire samples contained significantly more CuO/TiO_2 (0.007 ± 0.001) than bulk samples (0.004 ± 0.0001). This is illustrated in fig. C.27c) in appendix C.

Table 2: Overview of the differences in elemental composition (normalized with TiO_2) between the sample groups. Chi-squared test found no difference between groups for potassium, even though $p < \alpha$. For germanium on the other hand, fire samples differed from bulk samples albeit p was slightly $>\alpha$.

Element	p (Kruskal-Wallis)	Chi-squared ($\alpha = 0.05$)
SiO_2/TiO_2	0.01	fire samples different from samples below fire
K_2O/TiO_2	0.04	no difference
V_2O_5/TiO_2	0.047	fire samples different from samples below fire
Cr_2O_3/TiO_2	0.01	bulk samples different from samples below fire
CuO/TiO_2	0.002	fire samples different from all other groups
GeO_2/TiO_2	0.051	fire samples different from bulk samples

3.2. Total lipid extracts

Due to a mistake during extraction, a bulk sample from block 5 (labcode 213B19DB16) had to be excluded from TLE analysis. The extraction for this sample was repeated to analyze *n*-alkanes but the amount of TLE was not determined in the second run. Lipid extract yields (normalized to TOC content) varied between 6 mg g^{-1} TOC (fire horizon in block 3) and 40 mg g^{-1} TOC (rhizosphere sample in block 4), averaging at 19 ± 1 mg g^{-1} TOC. If yields were normalized to sample weight, they ranged from 23 µg g^{-1} to 118 µg g^{-1} and averaged at 53 ± 4 µg g^{-1}. There was no significant difference in TLE contents between blocks. This was true if extracts were normalized to TOC ($p = 0.79$), and if they were normalized to sample weight ($p = 0.16$).

There was however a significant ($p = 0.001$) difference between groups for TLE yields normalized to TOC with fire horizons containing significantly lower amounts than rhizosphere ($p = 0.001$) and bulk ($p = 0.02$) samples. Contents were lowest in fire horizons (8 ± 1 mg g^{-1} TOC), followed by samples above and below fire horizons (11 ± 2 and 16 ± 3 mg g^{-1} TOC, respectively) and bulk samples (21 ± 2 mg g^{-1} TOC). Rhizosphere had the highest yields with 31 ± 5 mg g^{-1} TOC. This pattern can also be observed in fig. 15.

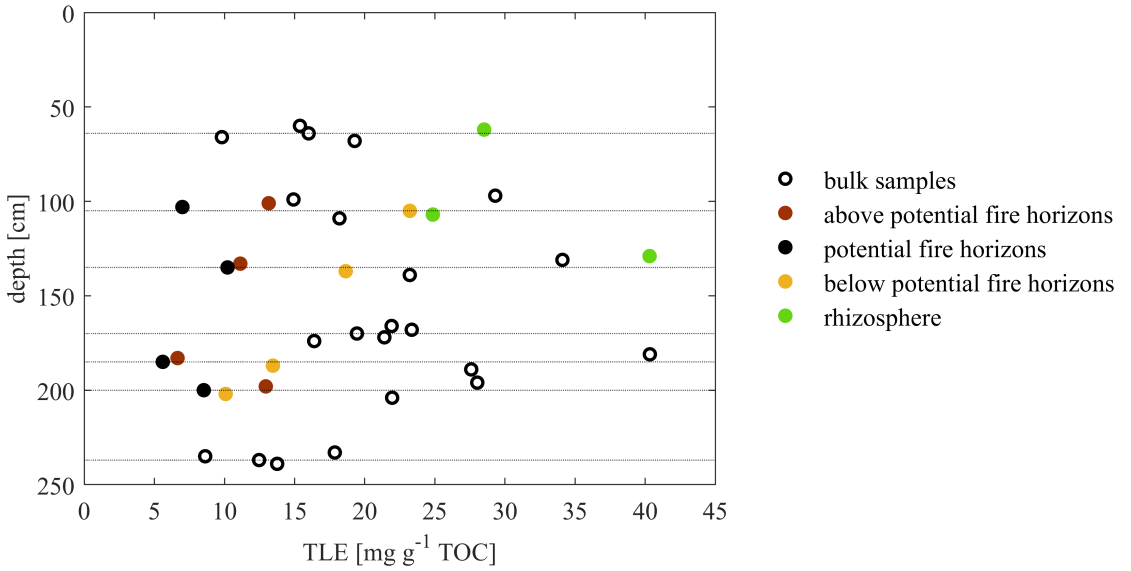

Figure 15: Measured TLE yields normalized to TOC. The dashed lines represent the depth in the middle of each block. Sample types are marked with different colored signatures.

A similar picture emerged when yields were normalized to sample weight. Contents varied significantly ($p = 0.02$) between sample groups, with rhizosphere samples containing significantly more than all other groups. Samples above and below fire horizons now exhibited the lowest yields (43 ± 8 and 47 ± 8 µg g^{-1}, respectively), while fire horizons had slightly higher contents (49 ± 4 µg g^{-1}), almost equal to bulk samples (51 ± 5 µg g^{-1}). Rhizosphere still had the highest yields with 92 ± 15 µg g^{-1}.

3.3. Aliphatic hydrocarbons

3.3.1. *n*-alkane contents

For all samples, *n*-alkanes with 16 to 33 C atoms were discovered. The average *n*-alkane concentration (normalized to TOC) was 174 ± 11 µg g^{-1} TOC. It varied between 61 µg g^{-1} TOC and 340 µg g^{-1} TOC. ANOVA and F-test revealed that block 5 was significantly different ($p = 0.004$) from blocks 6 and 7. There was no linear correlation between *n*-alkane concentrations and depth, both when fire horizons were included ($R^2 = 0.01$) and excluded ($R^2 = 0.03$). This indicates the absence of a depth-dependent decrease of the alkane content. The different blocks contained the following total amounts of *n*-alkanes (fig. 16a): Block 1 (at the bottom): 638 µg g^{-1} TOC, block 2: 903 µg g^{-1} TOC, block 3: 767 µg g^{-1} TOC, block 4: 1065 µg g^{-1} TOC, block 5: 1523 µg g^{-1} TOC, block 6: 962 µg g^{-1} TOC, and block 7: 737 µg g^{-1} TOC. Generally, *n*-alkane amounts varied little within single blocks. However, as can be observed in fig. 16a, the intra-block variability was strong in blocks 2 and 3. This is mostly owed to very low concentrations in and around the fire horizons and comparatively rather large concentrations in the bulk samples. In blocks 5 and 6, which both also contain a fire horizon, *n*-alkane concentrations were generally lower. Thus, the difference between the concentration in and around fire horizons compared to the bulk samples was not as pronounced leading to lower standard errors.

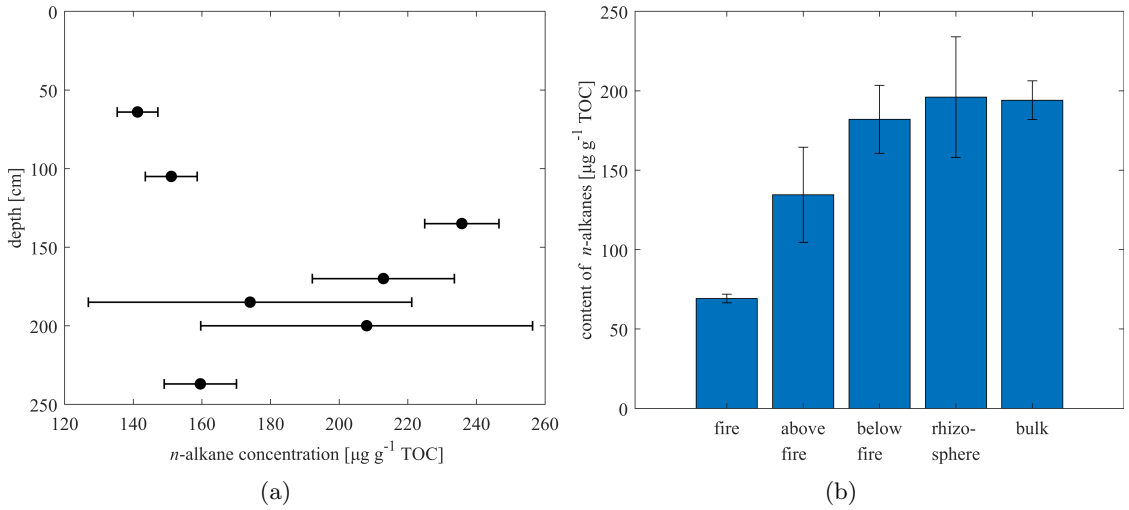

Figure 16: Average *n*-alkane concentrations normalized to TOC for the blocks (a) and sample groups (b) with error bars representing the standard error of the mean.

Also noticeable is the high standard error in block 4, which is due to two bulk samples with comparatively low alkane contents. There was no obvious characteristic, which would explain the smaller alkane concentrations of these samples.

When sample groups were compared, a clear picture emerged (fig. 16b). Fire horizons had by far the lowest *n*-alkane concentrations with 69 ± 3 µg g^{-1} TOC, followed by samples above and below fire horizons (135 ± 30 and 182 ± 21 µg g^{-1} TOC, respectively). Average concentrations in bulk (194 ± 12 µg g^{-1} TOC) and rhizosphere (196 ± 38 µg g^{-1} TOC) samples were almost identical. ANOVA showed that *n*-alkane yields varied significantly ($p = 0.003$), with samples from fire horizons containing substantially lower amounts than all other groups except samples above fire horizons, where the difference was not statistically significant ($p = 0.5$). This is also illustrated in fig. 16b.

If total *n*-alkane concentrations were normalized to sample weight, there was no statistically significant difference between sample groups ($p = 0.6$). Alkane concentrations ranged from 312 ng g^{-1} to 763 ng g^{-1} (both found in bulk samples from block 2), with an overall average of 481 ± 78 ng g^{-1}. The fact that block 2 contained both the sample with the highest and the lowest *n*-alkane concentration normalized to sample weight, was also evident in the high standard error of this block (514 ± 95 ng g^{-1}). There was a statistically significant difference between the blocks ($p = 0.04$) with block 3 containing substantially more *n*-alkanes (602 ± 50 ng g^{-1}) than block 7 (345 ± 13 ng g^{-1}).

Short-chain n-alkanes

When comparing the amount of short-chain (<20 C) *n*-alkanes (normalized to TOC), amounts varied significantly between sample groups ($p = 0.0002$) with fire horizons containing significantly less than bulk ($p = 0.0002$) and rhizosphere samples ($p = 0.005$) and rhizosphere samples containing more short-chain alkanes than all other groups. It did not differ significantly between blocks ($p = 0.3$). As summarized in Certini 2005, an increase in the relative contribution of short-chain alkanes is reported after fire. Results show however, that the ratio of short (<20 C) to long-chain compounds (21 to 33 C) was not significantly different among groups ($p = 0.09$). Linear regression analysis revealed that

the ratio decreased moderately with depth ($R^2 = 0.5$). There was a significant difference in the short to long-chain ratio between blocks (p = 3.3e-06). Post-hoc F-test revealed a significant difference between the short vs. long-chain ratio of block 7 and all other blocks below. The ratio in block 6 was also significantly higher than the one from blocks 1 and 2. ANOVA showed that the short-chain alkane content did not differ among blocks (p = 0.1) but that there was a significant (p = 0.003) difference in the long-chain alkane content between blocks. Blocks 6 and 7 both had significantly less long-chain alkanes than block 5. Additionally, block 7 had less long-chain alkanes than block 2. It therefore seems that the moderate decline in the short to long-chain ratio with depth as indicated by linear regression analysis is due to a relative enrichment in long-chain rather than a relative depletion in short-chain compounds towards the bottom of the profile.

n-alkane chain length distribution

In all blocks the alkane concentrations for short-chain alkanes peaked at C_{18}. The maximum for long-chain alkanes was at C_{29} in blocks 6 and 7 at the top of the profile (younger), while at the blocks towards the bottom (1 to 4) the maximum alkane concentrations were reached at C_{31}. In block 5, a shift occurred at the sample below the fire horizon. Until and including this sample, the peak was at C_{29}, while from there on downwards in the soil profile the maximum was at C_{31}. Within blocks, the maximum concentration over all alkanes (16C - 33C) was identical to the maximum of the long-chain alkanes, except for block 7, where the overall maximum alkane concentration was at C_{18}. The maximum over all alkanes for the individual samples within a block, was generally always at the same alkane, regardless of sample type. Only in block 6, the maximum concentration was at a different alkane for the fire horizon and the rhizosphere sample (C_{18} for both) compared to the bulk material in the block (C_{29}). The average *n*-alkane chain length distribution for the single blocks is illustrated in fig. C.30 in appendix C.

Apart from lower amounts of *n*-alkanes in fire horizons, there were also some differences in *n*-alkane composition (normalized to TOC) between sample groups. A summary of the variations of the individual alkanes between the groups is provided in table 3. Most differences occurred between fire horizons and bulk samples as well as between rhizosphere and the other groups (especially fire). In these cases, fire horizons contained less of the respective alkanes compared to other groups. Interestingly, rhizosphere samples had substantially higher concentrations of short-chain alkanes, especially C_{18} and C_{19} than all other groups. As illustrated in fig. 17e, the concentration of short-chain alkanes even exceeded the amount of long-chain alkanes - a pattern that was only observed for rhizosphere samples.

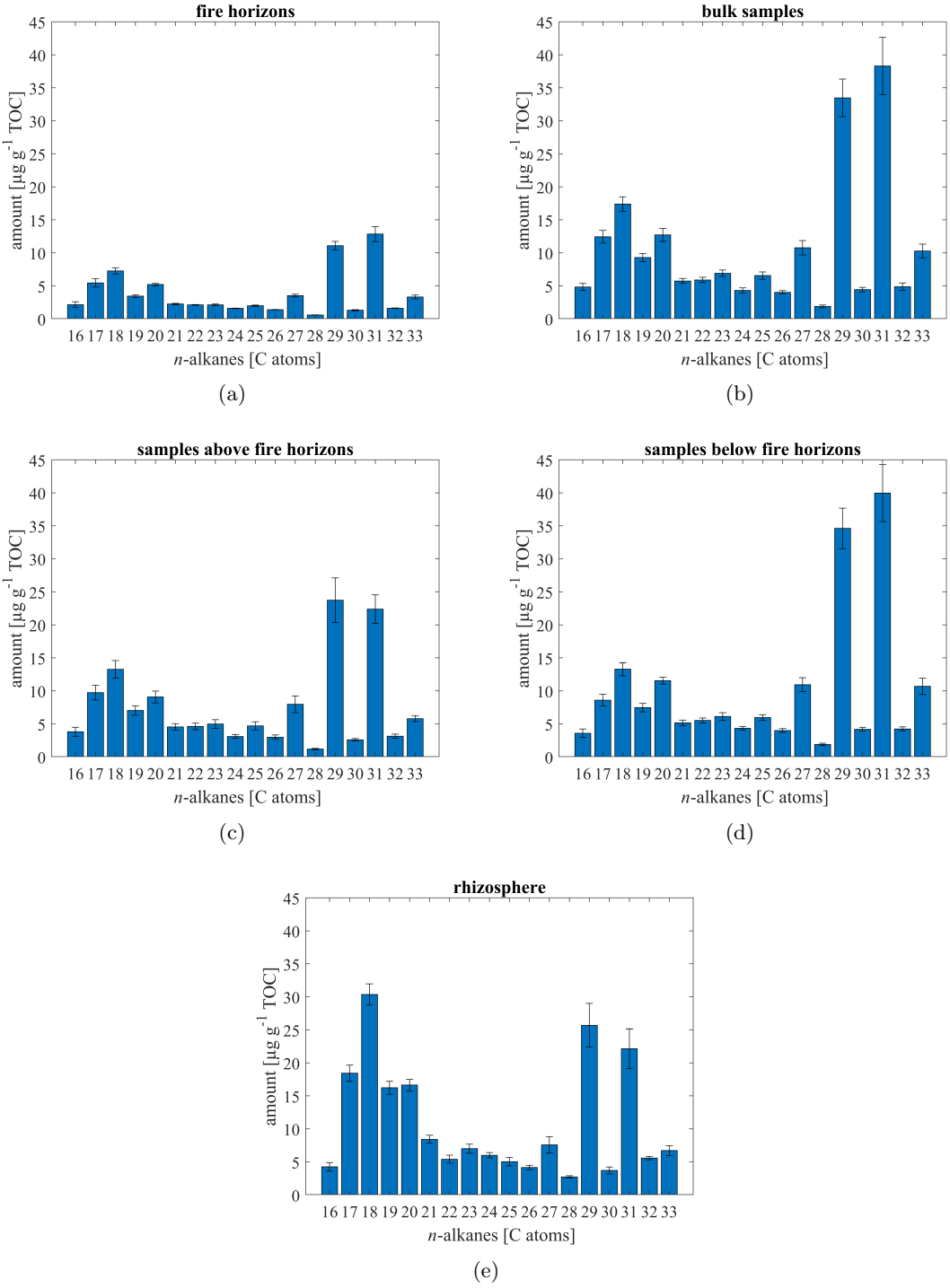

Figure 17: The alkane chain length distribution with the average of all detected *n*-alkanes for fire samples (a), bulk samples (b), samples above fire (c), samples below fire (d) and rhizosphere samples (e). Error bars represent the standard error of the mean.

Table 3: Overview of the differences in the individual *n*-alkane contents (normalized to TOC) between the sample groups.

n-alkane	p (ANOVA)	F-test ($\alpha = 0.05$)
C16	0.41	no significant differences
C17	0.01	fire different from rhizosphere
C18	2.51E-05	fire different from rhizosphere & bulk all different from rhizosphere
C19	4.64E-05	fire different from rhizosphere & bulk all different from rhizosphere
C20	0.01	fire different from rhizosphere & bulk
C21	0.001	fire different from rhizosphere & bulk
C22	0.02	fire different from bulk
C23	0.01	fire different from bulk
C24	0.01	fire different from rhizosphere & bulk
C25	0.03	fire different from bulk
C26	0.01	fire different from all except above fire
C27	0.10	no significant differences
C28	0.04	fire different from rhizosphere
C29	0.04	fire different from bulk
C30	0.01	fire different from bulk
C31	0.07	no significant differences
C32	0.09	no significant differences
C33	0.04	no significant differences

When *n*-alkane concentrations were normalized to sample weight, there were generally less differences in *n*-alkane composition between groups. Statistically significant differences between rhizosphere and all other groups were revealed for C_{17} ($p = 0.05$), C_{18} ($p = 0.0001$), and C_{19} ($p = 0.0001$), for which rhizosphere contained larger amounts. For C_{21}, there was also a significant ($p = 0.005$) difference between rhizosphere and all other groups except samples above fire horizons.

3.3.2. Pristane and phytane

Pristane and phytane contents normalized to TOC did not vary significantly between blocks ($p = 0.50$ and $p = 0.17$, respectively). A difference between groups could be detected for phytane ($p = 0.01$) but not for pristane concentrations ($p = 0.28$). Fire horizons had the lowest amounts (2 ± 0.4 µg g^{-1} TOC) of phytane, followed by samples below and above fire (4.7 ± 1 and 5 ± 2 µg g^{-1} TOC, respectively), bulk samples (7 ± 1 µg g^{-1} TOC), and rhizosphere (10 ± 2 µg g^{-1} TOC). Pristane concentrations displayed almost the same pattern with low concentrations for fire horizons (1 ± 0.2 µg g^{-1} TOC), followed by samples below and above fire (2 ± 0.4 and 4 ± 2 µg g^{-1} TOC, respectively), rhizosphere (4 ± 1 µg g^{-1} TOC), and bulk samples (4 ± 1 µg g^{-1} TOC). Overall, pristane and phytane concentrations averaged at 4 ± 1 and 6 ± 1 µg g^{-1} TOC, respectively. In several blocks, there were samples that had markedly high concentrations of either pristane and/or phytane (normalized to TOC). From the nature of these individual samples, it was not apparent how this unusual values came to be. As this is not of central relevance for answering the research question, I will not further investigate the reason for these values.

If concentrations were normalized to sample weight, pristane contents ranged from 2 - 37 ng g^{-1} (average of 10 ± 1 ng g^{-1}), phytane varied between 6 - 35 ng g^{-1} (average of 17 ± 1 ng g^{-1}). Pristane yields did not differ significantly ($p = 0.64$) between groups. Bulk samples and rhizosphere samples had similar amounts (11 ± 2 ng g^{-1}, 12 ± 3 ng g^{-1}, respectively), followed by samples above (11 ± 5 ng g^{-1}) fire horizons, fire horizons (8 ± 1 ng g^{-1}) and finally samples below fire horizons (6 ± 1 ng g^{-1}). For phytane, rhizosphere samples (29 ± 4 ng g^{-1}) contained more ($p = 0.03$) than all other groups except samples above fire horizons (18 ± 2 ng g^{-1}). Concentrations in fire horizons, samples below fire horizons and bulk samples were 15 ± 1 ng g^{-1}, 14 ± 3 ng g^{-1}, and 16 ± 1 ng g^{-1}, respectively. While for pristane, there were no difference between blocks, the amount of phytane was higher in block 3 than in blocks 1 and 2 ($p = 0.01$).

3.3.3. ACL and CPI

ACL ranged from 22 to 28 with an average of 25 ± 0.2. CPI values varied between 3 and 14, averaging at 6 ± 0.4. It was found that both ACL and CPI increased with depth. Linear regression analysis produced an $R^2 = 0.6$ for both, which corresponds to a moderate effect size (Moore *et al.* 2013). This tendency was not found for CPI_{short}. ANOVA revealed significant differences between blocks for ACL ($p = 1.6e\text{-}06$) and CPI ($p = 1.8e\text{-}06$). Neither ACL nor CPI and CPI_{short} differed significantly among sample types.

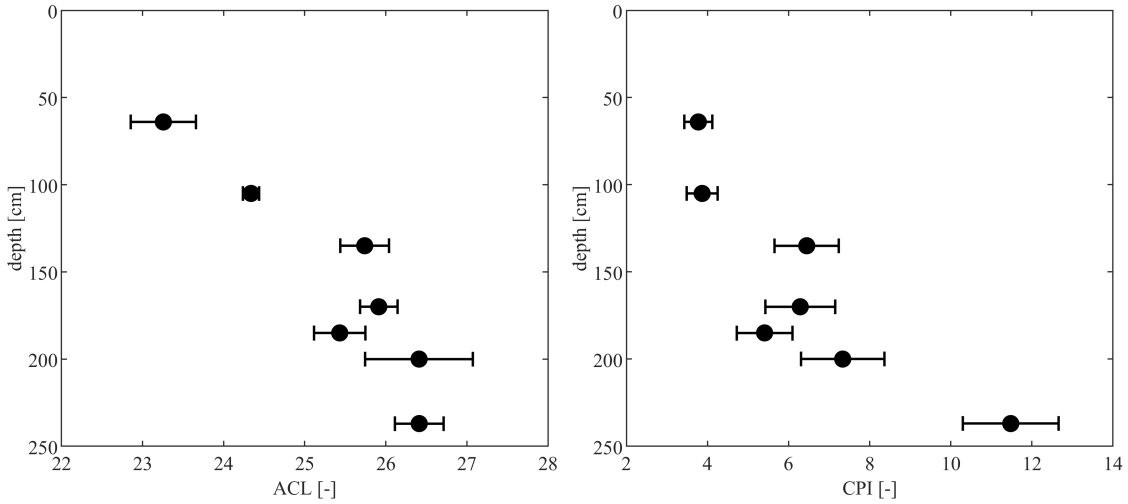

Figure 18: Average ACL (a) and CPI (b) increased with depth. Error bars represent the standard error of the mean.

3.3.4. Ratio of C_{27}/C_{31} alkanes

Over all samples, the ratio of C_{27}/C_{31} ranged from 0.14 to 0.49 (average 0.30 ± 0.01). It was found that it decreased slightly with depth ($R^2 = 0.3$), i.e. with increasing age of the OM (fig. 19). ANOVA showed a significant ($p = 0.001$) difference between blocks. The ratio was significantly higher in block 5 compared to blocks 1 to 4 and the ratio in block 7 was significantly higher than in block 3. Among sample groups there was no significant difference ($p = 0.9$).

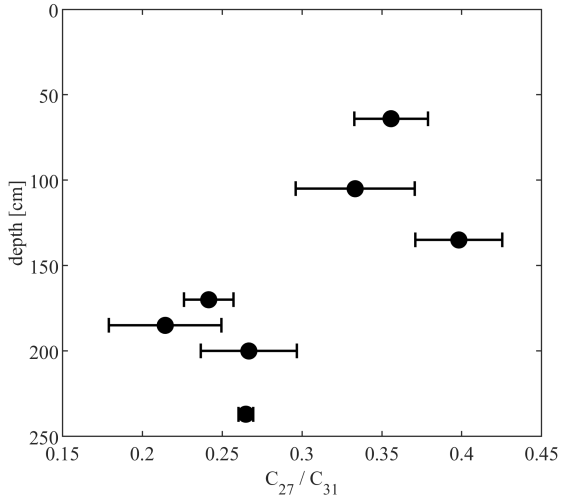

Figure 19: The average ratio of C_{27}/C_{31} alkanes changed with depth, i.e. age of the organic matter. Error bars represent the standard error of the mean.

3.4. BPCA concentration and composition

BPCA-C yields correlated moderately with TOC ($R^2 = 0.6$). They varied between 13 (bulk sample in block 7) and 183 g kg^{-1} TOC (charcoal piece) with an average of 41 ± 5 g kg^{-1} TOC. Kruskal-Wallis test revealed no significant difference between the blocks ($p = 0.07$). For an illustration of the BPCA-C concentrations plotted against depth see fig. C.31 in appendix C. Apart from the fire horizons, where higher BPCA-C concentrations were expected, there were some other samples that were characterized by comparatively high BPCA-C yields. Generally, rhizosphere samples were found to exhibit higher concentrations than bulk samples (44 ± 16 and 25 ± 2 g kg^{-1} TOC, respectively) yet not enough to reach statistical significance ($p = 0.74$). This is due to the high standard error of rhizosphere samples, which in turn was caused by a low BPCA-C concentration of the rhizosphere sample in block 7 (18 g kg^{-1} TOC). With a value of 183 g kg^{-1} TOC, i.e. more than seven fold the average concentration found in bulk samples, the charcoal piece had by far the highest concentrations of BPCA-C. Contrary to the blocks, BPCA-C yields differed significantly ($p = 0.004$) between groups. A Chi-squared test revealed that all groups exhibited lower BPCAs yields than fire (89 ± 14 g kg^{-1} TOC). After fire horizons, samples below and above fire horizons had the highest concentrations of BPCA-C (47 ± 15 and 37 ± 7 g kg^{-1} TOC, respectively). The average BPCA-C concentrations for the sample groups are shown in fig. 20

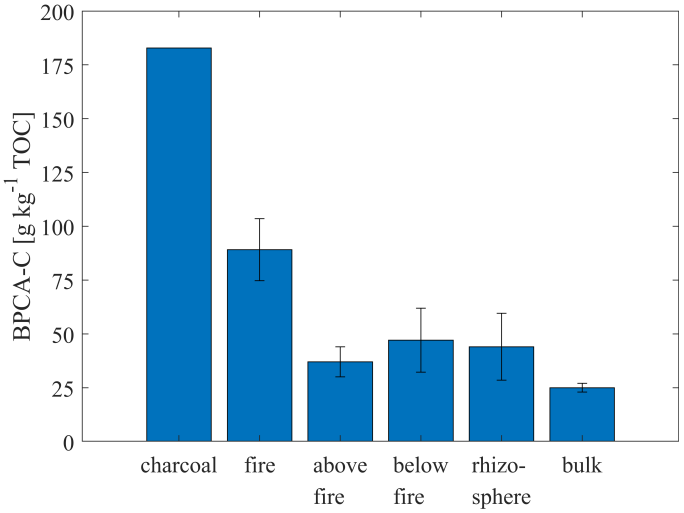

Figure 20: BPCA-C concentrations for the sample groups. The charcoal piece extracted in block 4, which was not included in any sample group, is shown for comparison. Error bars represent the standard error of the mean.

BPCAs were present as hemimellitic acid and trimellitic acid (B3CA), pyromellitic, mellophanic and prehnitic acids (B4CA), benzene-pentacarboxylic acid (B5CA), and mellitic acid (B6CA). As apparent in fig. 21, the relative contributions of the individual BPCAs did not differ significantly between groups.

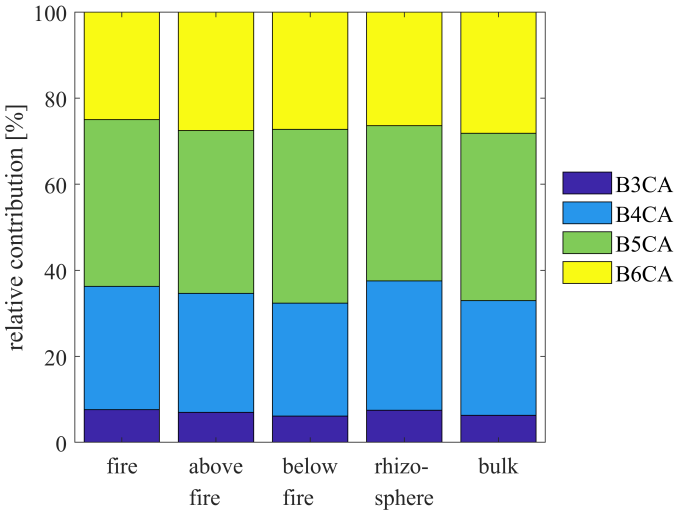

Figure 21: The relative contributions of the individual BPCAs did not differ significantly between sample types.

The ratio of B5CA/B6CA as a measure for the degree of aromatic condensation did not differ significantly between groups ($p = 0.94$). When comparing the individual fire horizons, it was highest for fire 2 (3.2), followed by identical ratios for fire 5 and charcoal (1.4). B5CA/B6CA for fire 6 was 1.1 and 0.9 for fire 3. Higher values indicate a higher contribution of B5CA compared to B6CA, i.e. values <1 indicate a higher amount of B6CA than B5CA. Because B6CA can only originate from the condensed core of BC, higher contributions of B6CA point to higher fire energy.

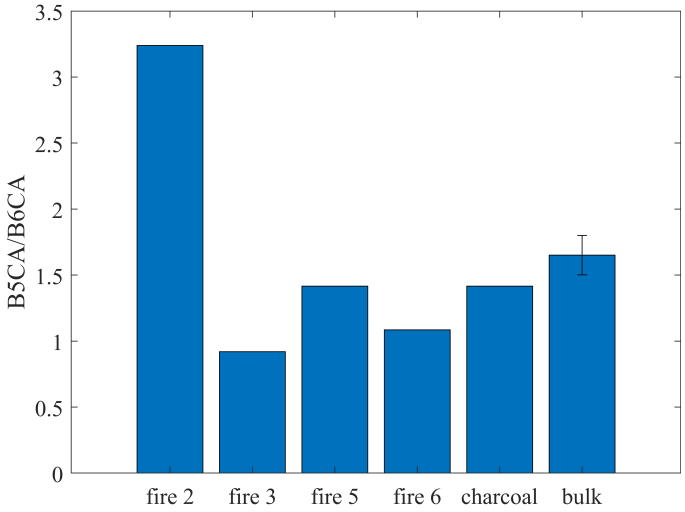

Figure 22: The ratio of B5CA/B6CA serves as a measure for the degree of aromatic condensation. It is shown for the four fire horizons as well as the charcoal sample and the average of the bulk samples for comparison. The error bar represents the standard error of the mean of the bulk samples.

4. Discussion

4.1. Evidence for a pyrogenic origin of the dark horizons

4.1.1. Color

What first led to the suspicion that the layers in blocks 2, 3, 5 and 6 may be fire horizons was their dark color. Indeed, studies have found a correlation between BC and a dark color of the soil (Wolf *et al.* 2014; Ulery & Graham 1993). Due to their recalcitrant nature, charred materials can persist in the environment and thus influence the color of the soil for a long time (Schmidt *et al.* 1999). Color was however only visually assessed and not classified using Munsell soil colors or by even measuring it with a spectrophotometer as done by Wolf *et al.* 2014 for example.

4.1.2. Black carbon

The concentration of BPCA-C, which serves as a marker for the original amount of aromatic moieties (Glaser *et al.* 1998), was found to be higher in the presumable fire horizons than in all the other groups. As can be inferred from table 4, fire 3, fire 5 and fire 6 had a BPCA-C concentration four times larger than the one of the average bulk sample. Fire 2 had comparatively low amounts with only half as much BPCA-C as the other fire horizons but still double the amount of the bulk horizons. Fire 2 is the oldest of the presumed fire horizons (roughly 28 ka cal BP). While BC is assumed to be hardly alterable in the environment (Schmidt & Noack 2000; Certini 2005), some studies have shown that, at least in certain environments, degradation can occur on a decadal to centennial timescale (Bird *et al.* 1999; Schmidt & Noack 2000). Nevertheless, there was no significant difference in the BPCA-C concentration between blocks and bulk samples in block 2 did not exhibit reduced amounts of BPCA-C. In fact, the bulk samples in block 2 contained 25 ± 2 g kg^{-1} TOC, which corresponds perfectly to the average over all bulk samples. This suggests that the lower yields of fire 2 are indeed due to its origin rather than the result of degradation. All in all, this supports the notion that these dark layers could indeed be the result of fire events.

Table 4: Overview of a selection of characteristics for the individual fire horizons. Fire 2 corresponds to the fire horizon in block 2, fire 3 to the one in block 3 etc. Block 2 was retrieved from the lower part of the profile, i.e. is older. For comparison, the charcoal piece and the average and standard error of the mean of the bulk samples are listed. *n.d.* = not determined

sample	TLE [mg g^{-1} TOC]	n-alkanes [µg g^{-1} TOC]	BPCA-C [g kg^{-1} TOC]	B5CA/ B6CA [-]	B6CA/ BPCA-C [%]	TOC [mg g^{-1}]	$\delta^{13}C$ [‰]	N [mg g^{-1}]
fire 2	9	71	47	3.2	13	7	-24.44	0.82
fire 3	6	71	102	0.9	36	7	-23.65	0.37
fire 5	10	74	110	1.4	26	5	-24.34	0.42
fire 6	7	61	99	1.1	31	7	-24.33	0.41
charcoal piece	*n.d.*	*n.d.*	183	1.4	21	11	-23.57	0.34
bulk samples	21	194	25	1.7	27	3	-25.55	0.33
	± 2	± 12	± 2	± 0.1	± 2	± 0.4	± 0.11	± 0.01

What was also quite noticeable, were the relatively high yields of BPCA-C in the rhizosphere samples. They were only slightly lower than concentrations in fire 2. There is a consensus among researchers that BC is solely produced by incomplete combustion (Glaser & Knorr 2008). Studies have however demonstrated that several methods used to quantify

BC, including the BPCA method, overestimate the amount of BC in soils, sediment and water (Glaser & Knorr 2008, Gerke 2019, Chang *et al.* 2018, Simpson & Hatcher 2004). A study by Glaser & Knorr 2008 suggested that up to 25 % of measured BPCA did not originate from fire but was produced in-situ. The same was found by Chang *et al.* 2018, who showed that organic matter can contain BPCAs without having been exposed to fire or charring. They also detected BPCAs in condensed OM of any kind, for example in humic acids (Chang *et al.* 2018). The main culprit for this overestimation seems to be that the BPCA method (and other common methods) measures polycyclic aromatic carbon, which is a constituent of BC. Humic substances have a chemically similar structure as BC. Hence, a fraction of the carbon from their aromatic structure is detected as BPCA and erroneously taken to indicate the presence of BC (Gerke 2019). This methodological artifact (Simpson & Hatcher 2004) of the BPCA method might be the reason, why the rhizosphere samples contained comparatively high concentrations of BPCA-C. Since humic acids are known to enhance root growth (Mora *et al.* 2012), it is plausible that this effect would be most pronounced in rhizosphere samples.

4.1.3. Carbon isotopic signature

Isotope values were in a range that is typical for C_3 plants (Ballentine *et al.* 1998). Several authors have found that a relative enrichment of ^{13}C occurs when C_3 vegetation is thermally degraded (e.g. Turekian *et al.* 1998; Wiesenberg *et al.* 2009). This can be explained by the fact that C_3 plants favor the decomposition of compounds with lighter isotope values (Wiesenberg *et al.* 2009). The described isotopic fractionation leading to higher $\delta^{13}C$ was also observed in the analyzed fire horizons. On average, isotope values of fire horizons increased by 1.4 ‰ compared to the mean of the bulk samples (table 4).

4.1.4. Lipid and *n*-alkane content

Amounts of TLE normalized to TOC lay within the typical range for soils described by Stevenson 1982 (20 - 60 g kg^{-1} of soil OM). If yields were normalized to sample weight, they were in the range of what has been reported for loess in Gocke *et al.* 2010. The same study found that loess in the proximity (0 - 5 cm) of rhizoliths ("a particular form of secondary $CaCO_3$ formed by encrustation of plant roots", Gocke *et al.* 2010) exhibited higher amounts of TLE. Even though the samples analyzed here did not contain rhizoliths, the rhizosphere samples were also taken in the immediate vicinity of roots and displayed elevated concentrations of TLE as well.

As summarized in Eckmeier & Wiesenberg 2009, fire can lead to an increasing or a decreasing abundance of TLE. In their experiment, Eckmeier & Wiesenberg reported lower amounts of TLE, which they suggested was due OM that had been depleted of lipids by at least one fire event and was then incorporated into the soil. In contrast, it has been demonstrated that charring at low temperatures (300 °C) can lead to a loss of biomass, which results in a relative enrichment of the lipid content (Wiesenberg *et al.* 2009). If temperatures were increased further (400 - 500 °C), more stable compounds (e.g. esters) started to degrade, leading to decreased lipid yields. The authors expected that at very high temperatures even lipids would start to degrade or to condense to BC or other aromatic structures. These observations might explain why fire horizons and bulk samples had almost identical amounts of TLE when normalized to sample weight. On the other hand, since fire horizons were enriched in C compared to bulk samples, fire horizons exhibited depleted TLE yields when normalized to TOC.

Concentrations of *n*-alkanes (normalized to TOC) were almost three times lower in fire horizons than in bulk samples. This is likely owed to the same reasons as discussed above, i.e. increased amounts of TOC, which led to a relative depletion of total *n*-alkanes. Compared to the average amount of *n*-alkanes in the bulk samples of the respective blocks, alkane concentrations (normalized to TOC) in the fire horizons were reduced by the following magnitudes: fire 2: -71 %, fire 3: -58 %, fire 5: -71 % and fire 6: -53 %. The high depletion in fire 2 is however partly owed to a very high alkane content in the bulk sample clearly below the fire horizon. If this sample is excluded for the calculation of the block's mean alkane content, the depletion of fire 2 relative to the bulk samples is slightly lower (-63 %). When contents were normalized to sample weight, no difference was detected in the alkane content between groups.

4.1.5. Summary: fire or no fire?

Overall, all the markers discussed above indicate that, most likely, the dark layers in blocks 2, 3, 5 and 6 were indeed exposed to fire. In some cases, the combustion traces were not restricted to the fire horizons but expanded to the samples above and below. This can be partly explained by the sampling as the delineation of the fire horizons was not always clear. However, this points to the second issue, which is mixing of the soil material (e.g. Wolf *et al.* 2014). Mixing can occur both over a small or large (e.g. by wind) spatial scale and caused similar but attenuated tendencies for the samples around the fire horizons. This made it more challenging to visually delimit the fire horizon. In the sample below the fire horizon in block 3 for example, amounts of BC, TOC and δ^{13}C were elevated compared to the bulk material, while TLE was lower - the same pattern as observed in the fire horizon but less pronounced. If this was caused by mixing of the soil sediment, it could also explain why the combustion traces in this block were only visible as a slight but not very prominent dark coloration (see fig. 8).

4.2. Fire energy

4.2.1. Black carbon content and composition

Larger contributions of B6CA to total BPCA-C indicate a higher degree of aromatic condensation and reflect higher energy input, i.e. charring temperatures (Schneider *et al.* 2010; Budai *et al.* 2017; Wolf *et al.* 2013). Schneider *et al.* 2010 found that the proportion of B6CA was <10 % at low charring temperatures (200 °C), increased to 10 – 40 % at moderate temperatures (250 – 500 °C) and reached contributions of >40 % at temperatures between 600 – 1000 °C. The same was reported by Budai *et al.* 2017, who demonstrated that B6CA became dominant at temperatures exceeding 600 °C. Fire 2 had the lowest contribution of B6CA (13 %), while the proportion of B6CA was more than double in fire 5 (26 %), fire 6 (31 %) and fire 3 (36 %). These relative contributions point to temperatures in the range of 250 – 500 °C for all fire horizons, though fire 2 was likely exposed to temperatures at the lower end of this range. This is in line with what is indicated by BPCA-C concentrations, which have been shown to increase with rising charring temperatures. Fire horizons in blocks 3, 5 and 6 contained similar amounts of BC, while the one in block 2 had a much lower concentration (table 4). This further supports lower thermal energy exposure of fire 2. Nevertheless, quantities of BC can be "diluted" by mixing of the soil sediment. Therefore, caution needs to be applied when drawing conclusion about fire energy from BPCA-concentrations alone.

While BPCA composition is not directly affected by the fuel type, it does have an indirect impact as combustion temperatures depend on the material that is being burnt (Wolf *et al.* 2013). Wolf *et al.* 2013 performed a literature review and distinguished three typical fire regimes (median ± standard deviation): grass and forest ground fires (285 ± 143 °C), shrub fires (503 ± 211 °C) and domestic fires (797 ± 165 °C). They reported a linear correlation between charring temperature and B5CA/B6CA and identified values of 0.8 - 1.4 as indicative for grass fires, 1.3 - 1.9 for forest ground fires, <0.8 for domestic fires and 0.8 - 1.7 for shrub fires. As can be inferred from table 4, fire 3 had the lowest ratio (suggesting the highest charring temperature), followed by fire 6, fire 5 and finally fire 2. All fire horizons except the latter lie within the ranges for shrub and grass fires, fire 5 also in the range for forest ground fires. Fire 2 has an extremely high ratio of B5CA/B6CA, which does not fit into the range of any of the described regimes. This might suggest that the fire was "cold". Likely, grass served as fuel since it reportedly burns at temperatures as low as 82.5 °C, especially when fuel is scarce (Stinson & Wright 1969; Bailey & Anderson 1980).

The charcoal piece had a B5CA/B6CA ratio of 1.4, which is in the range of forest ground and shrub fires, as well as on the margins for grass fires. BPCA-C concentrations were very high compared to the bulk samples. This does however not imply higher charring temperatures, since this is due to it being a charcoal piece while the fire horizons were soil sediment material enriched in BC. Rather, the proportion of B6CA and B5CA/B6CA suggest a similar charring energy as for fire 5.

4.2.2. TOC and carbon isotopic signature

Fire horizons had more TOC, which is expected as TOC is successively enriched with increasing thermal degradation (Wolf *et al.* 2013; Wiesenberg *et al.* 2009). For soft- and hardwood it has been demonstrated that an increase in TOC only occurs if temperatures reach more than 150 °C (Czimczik *et al.* 2002). Whether this minimum temperature for enrichment of TOC also exist for grass vegetation, which was probably an important fuel, I could not find out. Because grass differs from wood in the proportions of lignin and cellulose, i.e. its physical structure (Wolf *et al.* 2013), it is however likely that there would be a difference in a potential temperature threshold. Depending on the fuel type, charring residues contain more or less TOC, with lower amounts produced by grass fires (Wolf *et al.* 2013). Additionally, the burning of grass and herbaceous plants does not result in large quantities of charcoal particles (Eckmeier & Wiesenberg 2009). While some small charcoal pieces (e.g. in block 4) were present, they were not very abundant neither in the fire horizons nor elsewhere. This supports the supposition implied by the B5CA/B6CA ratio that the fires may have been grass fires or that at least, grass was an important fuel source for these fires.

In their study, Turney *et al.* 2006 looked at the isotopic signature of three different woods (*Eucalyptus* spp., *Quercus robur* and *Pinus radiata*) that they heated in a laboratory setting. They found that the shift in isotopic values depended on the temperature and the species but was reached after 30 min of heating, i.e. did not depend on heating duration. In contrast, Wiesenberg *et al.* 2009 did not detect further isotopic fractionation with increasing temperatures. Shifts in isotopic values of +1.2 ‰, +1.0 ‰, +1.5 ‰ and +1.1 ‰ for fires 2, 3, 5, and 6 compared to the average of the bulk samples of the respective block, are in the range of what has been reported for a C_3 grass (+1.3 ‰ for rye) at a charring temperature of 300 °C (Wiesenberg *et al.* 2009). Comparison with what was found by Turney *et al.* 2006, the results would point to higher temperatures of about

400 °C. This study was however conducted on different woods, while Wiesenberg *et al.* 2009 looked at grasses. It appears that the extent and the direction of the observed shift and whether it depends on charring temperature is, amongst other things, a function of the analyzed species.

4.2.3. *n*-alkane chain length distribution

Studies have repeatedly described a relative enrichment of short-chain alkanes after exposure of biomass to fire (e.g. Almendros *et al.* 1988). In particular, an increase in even numbered, short-chain homologues maximizing at C_{16} or C_{18} was observed (Eckmeier & Wiesenberg 2009; Wiesenberg *et al.* 2009). This is also reflected in higher values for CPI_{short} with increasing thermal degradation (Wiesenberg *et al.* 2009). CPI and ACL on the other hand, decrease at high temperatures because the C bonds get destroyed (Wiesenberg *et al.* 2009). Investigations of Wiesenberg *et al.* 2009 indicate that the extent and type of change that occurs in the alkane pattern depends on the charring temperature. At 300 °C, alkane composition still largely resembled the one of primary plants, with a larger amount of mid-chain alkanes (19 - 25C) and a less pronounced relative predominance of even, long-chain alkanes. At 400 °C, even and odd alkanes were almost equally abundant (maximum at C_{22} for rye) and higher yields for pristane and phytane were measured. At 500 °C, long-chain alkanes were further reduced leading to a relative increase in even short-chain *n*-alkanes. The observed differences in individual alkane concentrations between sample groups (table 3) are the result of generally lower amounts of alkanes in fire horizons. The lack of a relative increase in the amount of short- vs. long-chain *n*-alkanes in fire horizons is explained by an equal depletion of both long and short-chain alkanes. This suggests that none of the fire horizons were exposed to high temperatures. Thus, original primary plant distribution patterns were preserved. Also, there was neither a significant increase in CPI_{short}, nor a significant decrease in ACL and CPI for the fire horizons compared to the bulk samples. CPI_{short} was only elevated in fire 3 (+42 % compared to the average of the bulk samples in this block) but not in the other ones. While a decrease in ACL did occur in fires 2, 5 and 6, it was small: -9 %, -4 %, -4 %, respectively compared to the average of the bulk samples in the respective block. For CPI, a decrease of -41 % was observed for fire 2 relative to the average of the bulk samples in the block. At temperatures of 300 °C, Wiesenberg *et al.* 2009 observed reductions in ACL of -9 % and of -76 % in CPI for rye grass. CPI_{short} for the rye straw was not determined so that the change in CPI_{short} is not known. Comparison of these reductions with the ones found here illustrates the generally small effect observed here. Only the reduction in the ACL of block 2 was in the same magnitude as in Wiesenberg *et al.* 2009. I would therefore argue that temperatures were likely not well above 300 °C. Temperatures below 400 °C are furthermore supported by lower concentrations for pristane and phytane in the fire horizons compared to the bulk samples - independent of whether they were normalized to sample weight or TOC.

As mentioned in the methods section, polycyclic aromatic hydrocarbons PAH were not measured because initial measurements revealed very low concentrations. Nevertheless, these first results showed that trace amounts of PAH were present in the fire horizons. Wiedemeier *et al.* 2015 found that straw material that had been exposed to a maximum temperature of 300 °C contained some PAHs, while in the untreated straw PAHs were not detected. PAHs increased further with higher temperatures. This suggests that the material in the fire horizons was exposed to heating but that temperatures were low.

4.2.4. Summary

Taking into account all the analyses discussed, it seems reasonable to conclude that all fires were low-energy. The results do however not allow the determination of the exact charring temperatures for the individual fire horizons. The observed shifts in δ^{13}C and the alkane compositions that were very similar to primary plant lipid distribution patterns, indicate temperatures around 300 °C. B5CA/B6CA did not prove to be very helpful to further narrow down the temperature range, as the values attributed to the different fire regimes overlap. Consequently, based only on the ratio B5CA/B6CA and the complete temperature ranges identified by Wolf *et al.* 2013 in their literature survey, fire 5 for example could have been exposed to charring temperatures anywhere between 82.5 °C and 1042 °C. What can however be concluded from B5CA/B6CA is that it is very unlikely that any of the fires were domestic fires, i.e. campfires. The relative contribution of B6CA to total BPCA-C puts all fire horizons in a temperature range of 250 - 500 °C, although fire 2 was most likely at the lower end or even below this range. In conclusion, the data suggests that all fire horizons were most likely not exposed to temperatures well above 300 °C. It is therefore probable that grass was a major contributor of the fuel for burning. Considering the relative proportions of B6CA, one might suspect that fire 3 was exposed to the highest temperatures, followed by fire 6, fire 5 and finally - well behind - fire 2. The presumably lowest fire energy in the latter, might have been due to limitations in oxygen supply and/or the quantity and quality of fuel.

4.3. Fires and human occupation

Human activities such as settlement and agriculture and societal change highly influence fire regimes, which in the past and present has often led to increasing emissions of BC into the environment (Thevenon *et al.* 2010). As outlined, it is unlikely that any of the fire horizons originated from domestic fires since these typically reach fairly high temperatures due to constant fuel supply (Wolf *et al.* 2013). Nevertheless, if the fires were not campfires, it doesn't necessarily mean that humans were not at play. Humans have for example used slash-and-burning in the context of so called shifting cultivation for thousands of years (Ponomarenko *et al.* 2019). The horizontal expansion of the charring traces in blocks 3, 5 and 6 seems however too little, while in block 2 it appears too large to suggest that this was the case here. Additionally, if the fires had been provoked by humans for agricultural purposes one would expect to see a further downward reaching mixing of the burnt material with the material below, e.g. through ploughing. It therefore appears that the residues originated from naturally occurring wildfires. Furthermore, the quantities of BC in the bulk samples ("background signal") at BL III remained largely the same over time. Thus, human occupation does not appear to have been a major contributor to BC emissions in the region. Supposedly, the "background" BC that's present in all samples was deposited by wind (Wolf *et al.* 2013). Although the fires were probably not directly related to human activity, the artifact (blade) recovered in block 3 is a clear indicator of human presence in the region around 27 ka.

4.4. Chemical composition of fire horizons

4.4.1. Carbon

The presence of more TOC in the fire horizons aligns with what is described in the literature, where rising amounts of TOC have been reported after biomass burning (e.g. Turney *et al.* 2006; Certini 2005). Wolf *et al.* 2014 hypothesized that the former land surface was most susceptible to input of OM and therefore also BC (burnt OM) input. Due to the recalcitrant nature of BC (e.g. González-Pérez *et al.* 2004), the enrichment of TOC is preserved for long time spans and can thus still be detected today.

4.4.2. C/N ratio and nitrogen

Studies have reported a decreased C/N ratio in the burnt soil due to accumulation and preferential preservation of N (Almendros *et al.* 2003; Mastrolonardo *et al.* 2014). In contrast, the results here showed an increase of the C/N ratio in the fire horizons. This was caused because both C and N contents were elevated but the enrichment of C exceeded the one of N.

The increased amount of N in the fire horizons provides further evidence for low-energy fires. This is due to the fact that N persisted in the soil rather than having been lost by volatilization, which is the most important mechanism for N loss during fire. Significant losses of N (over 50 %) occur when temperatures exceed 300 to 400 °C. Below temperatures of 200 °C, no N is lost (Beyers *et al.* 2005). At temperatures between 200 to 300 °C, much of the N can be preserved in inorganic forms that result during heating (Beyers *et al.* 2005; Knicker *et al.* 1996). These inorganic forms are ammonium (NH_4^+), which is a direct result of burning, and nitrate (NO_3^-), which forms from ammonium some time after fire (Certini 2005). Both N forms are bio-available but can be leached (nitrate) or held by the soil (ammonium), if they are not taken up by plants (Beyers *et al.* 2005; Certini 2005). However, if ammonium is not fixed within the structure of clay minerals, nitrification will occur (Certini 2005). The loamy soil and sediment at BL III might therefore explain, why the N content in the fire horizons is still significantly increased even thousands of years post-fire. One could speculate that a potentially higher proportion of clay in the lower part of the profile is also the reason why twice as much N was present in fire 2 compared to the other fire horizons as more ammonium could be preserved in the interlayer of clay minerals. Nevertheless, the grain size distribution throughout the profile was not investigated. Additionally, the suspected lower fire temperatures in this horizon might have further limited the loss of N through volatilization during burning.

4.4.3. Other elements

Most statistically significant differences between sample groups did not occur between fire horizons and other groups. However, differences between the fire horizons and the samples below can also be revealing. Research has shown that most elements leached from above can be held, i.e. accumulated, in the layers that were not exposed to thermal shock (Certini 2005). Potentially, this could explain higher concentrations of Si and V in samples below fire horizons compared to the fire horizons as well as the increased amount of Cr below fire horizons as opposed to the bulk material. Cu was the only element with statistically significant different (higher) concentrations in fire horizons compared to all other groups. Unfortunately, studies investigating the effect of fire on the behaviour of elements such as Cu, Fe, Mn and Zn are scarce (Certini 2005). Different forms of Mn have been found to

be elevated post-fire. The same behaviour is assumed for Cu, Fe and Zn, which are hardly leached and could therefore be enriched in burnt soil (Certini 2005). A study conducted in a mountain region in Serbia, compared soils approximately 1 year after a wildfire that lasted for 10 days with undisturbed soils in the region (Stankov Jovanovic *et al.* 2011). They found higher amounts of the studied elements Cu, Pb, Cd and Zn in the burnt soil. Since the highest elevations were reported in the amounts bound to oxides and organics and only to a lesser degree in the bio-available forms, it is possible that these fire-induced increases could be preserved for a long time.

When looking at the behaviour of P in the analyzed samples, a slight but not statistically significant increase in the fire horizons compared to the bulk samples can be observed. As P volatilizes at a temperature of 770 °C (Beyers *et al.* 2005), it is not easily lost in low-energy fires. It also appears that losses through downward movement, i.e. leaching, are not an issue (Certini 2005). Fire converts organic P to its bio-available form (orthophosphate), thus leading to an increase in P available to biota (Certini 2005). How long this enrichment of available P persists, depends on several factors and has been demonstrated to last for 21 months (Macadam 1987). Likely, any increase in orthophosphate does not survive for thousands of years, which suggests that the slightly higher P contents in the fire horizons are organic forms of P.

Fire also increases the availability of other soil nutrients apart from P and N (González-Pérez *et al.* 2004). For many nutrients, this increase does not last long however (Certini 2005). Smith 1970 for example, reported higher amounts in nutrients such as Na, K, Ca and others after fire but found that they had been depleted 15 months after the event. In fact, he observed the greatest leaching already during the first 3 months. The fire horizons analyzed here did not display significantly different amounts of these nutrients. However, in the burnt layers Na and K were present in slightly lower amounts, while Ca seemed to be slightly enriched. Nevertheless, considering that the fires happened several thousand years ago, it remains unclear as to whether these small changes can be attributed to them, especially since long-term studies are lacking.

4.4.4. Summary

All fire horizons were characterized by high amounts of TOC as well as higher concentrations of N and Cu and lower amounts of Si, V and Cr. Overall however, the elemental composition of fire horizons largely resembled the one of the bulk material and on its own would not be enough to distinguish fire horizons with confidence.

4.5. Plant wax lipids as a proxy for past vegetation dynamics

4.5.1. Variation in *n*-alkane composition throughout the profile

It has been observed that less resistant short- and medium (<C22) chain alkanes can be subject to selective degradation (Cranwell 1981; Jansen & Wiesenberg 2017). This did however not cause the high short to long-chain alkane ratio in the uppermost part of the profile. Rather, the decreasing ratio with depth was the result of elevated amounts of long-chain alkanes (>20C) instead of a depletion of short-chain alkanes. The increasing amount of long-chain alkanes is also the reason for the generally higher ACL values with depth. The lower input of long-chain alkanes in the top of the profile could be attributed to alkane input of below-ground biomass, i.e. roots. The epicuticular wax composition differs not only among species but also within parts of the same species (Eglinton &

Hamilton 1967). The amount and composition of wax lipids in roots can be different from the one in aboveground biomass (Jansen & Wiesenberg 2017). This difference between roots and leaves of a single plant can be in the same magnitude as the difference in the alkane composition of leaves between different species (Jansen & Wiesenberg 2017). The degree of influence of roots can be highly variable within the same profile depending on the depth (Angst *et al.* 2016). While roots were found almost throughout the profile, they seemed to have the highest impact on the *n*-alkane composition in the uppermost ∼100 cm below ground. Root extracts can have a larger relative contribution of alkanes with 16 – 20 C atoms than aboveground biomass (Jansen *et al.* 2006; Gocke *et al.* 2014). As outlined in the results section, rhizosphere samples indeed contained significantly more short-chain alkanes than all other groups. It might therefore be the case that roots, which incorporated a higher proportion of short-chain alkanes, were the main source of *n*-alkanes in the upper part of the profile, while the input of long-chain alkanes was limited. While low CPI values (<10) as reported here, are often indicative of a predominantly microbial origin of the OM (Cranwell 1981), they can also be related to root biomass (Gocke *et al.* 2010). Indeed, the higher amounts of C_{18} that were found in the rhizosphere samples might explain the lower odd over even predominance (indicated by CPI) in depths that were influenced by roots (Gocke *et al.* 2010). Nevertheless, ACL of long-chain alkanes (equation 2 with n in the range of 25 - 33C) with values >29 for all samples indicate that input from epicuticular leaf waxes of higher plants was important throughout the whole profile (Eglinton *et al.* 1962).

4.5.2. Vegetation change over time

There was no difference in TLE content between blocks, which indicates that the accumulation of waxes and thus the amount of biomass was similar throughout the whole time span represented by the profile. A dramatic shift in C_{27}/C_{31} between the upper and the lower part of the profile (fig. 19) indicates however a change in vegetation composition over time. This shift coincides with the onset of the LGM, which lasted from about 26.5 ka to 19 to 20 ka (Clark *et al.* 2009). At the onset of deglaciation in the northern hemisphere, no change in vegetation is evident by C_{27}/C_{31}. The ratio was ∼0.25 in the lower part of the profile and increased to ∼0.36 in the upper part of the profile. Values <1 result from a greater input of C_{31} relative to the input of C_{27}. The increase of the ratio around the onset of the LGM indicates that the relative abundance of C_{31} decreased at this time. This is in line with the maximum alkane concentrations that appear at C_{31} at the older part of the profile and at C_{29} in the younger section of the profile. As outlined in the results section, a shift of the maximum alkane concentration occurs within block 5 (max. at C_{31} in the older part, max. at C_{29} in the younger part). As this block was dated to 26.5 ka (table 1), this suggests that the climatic changes of the LGM and possible subsequent changes in vegetation are captured in the sedimentary record of the profile in BL III. As C_{27} and C_{29} are more abundant in tree vegetation (e.g. Schwark *et al.* 2002) and grass usually contains higher amounts of C_{31} (e.g. Lei *et al.* 2010), the shift in C_{27}/C_{31} could imply that grass vegetation was more predominant before 26 ka and that trees and shrubs were more abundant as the LGM set in. Values clearly <1 for all samples suggest that grass and herbaceous vegetation were always present. As proposed by Obreht *et al.* 2019, ratios such as C_{27}/C_{31} should be interpreted as the domination in their respective biomass, i.e. as an indicator for the relative contribution of grasses and herbs vs. trees and shrubs to total biomass production. A decrease in this ratio does therefore not necessarily imply a remarkable increase in trees and shrubs but rather a

decrease in grass and herb vegetation that might be attributed to climatic changes. The ratio has also been shown to decrease during decomposition and the formation of soil OM (Obreht *et al.* 2019). Buggle *et al.* 2010 even proposed that changes in C_{27}/C_{31} are rather the result of postsedimentary alteration effects than changes in palaeovegeation. Furthermore, variations of *n*-alkane chain length distributions in sediment archives seem to be driven by aridity and/or the temperature during the growing season (Bush & McInerney 2015). Studies report for example a connection between relative humidity and *n*-alkane chain length, which often leads to higher ACL under drier conditions (Schäfer *et al.* 2016). Changes of C_{27}/C_{31} over time can therefore be indicative of changes in climate rather than vegetation (Bush & McInerney 2015). It is hence not inconceivable that the observed shift in C_{27}/C_{31} reflects climatic changes at the onset of the LGM instead of changes in vegetational composition. Complementary investigations are thus necessary to reconstruct the palaeovegetation as *n*-alkane composition alone is not sufficient (Gocke *et al.* 2013). Fossil pollen in sediments, for example, are an important proxy for reconstructing changes in the palaeoenvironment (Sadori *et al.* 2016). In 1977, a study was published, where pollen records at Bistricioara-Lutărie I and two other sites in the Bistriţa Valley were investigated (Păunescu *et al.* 1977). Nevertheless, it has been convincingly shown that palaeoclimatic and archaelogical inferences for these sites are inaccurate and need to be revised (Schmidt *et al.* 2020). It has furthermore been demonstrated that pollen from archaeological sites are not reliable for vegetation reconstruction because they are influenced by human activities (Tomescu 2000, Danu & Bodi 2015). Another issue arises because loess deposits favor selective degradation of pollen (Tomescu 2000). Since loess and loess-derivates are common at Bistricioara-Lutărie I, results from pollen analysis of this site have to be taken with caution. These factors combined with oxic conditions in the soil at BL III (personal communication, G. Wiesenberg) make this site unsuitable for pollen analysis. Thus, in order to derive reliable information about the past environment, either pollen analyses of natural, loess-free settings or lake sediments (Tomescu 2000) in the region or the application of other molecular proxies are required.

There are no studies about palaeoenvironment in the Bistrița valley specifically but reconstructions of past vegetation and climate exist for the East Carpathians. Magyari *et al.* analyzed the sedimentary archive in a volcanic crater ∼140 km south of BL III and found an attenuated response to global cooling in the region. The record suggested boreal forest steppe vegetation in the foreland and low mountain zones during the LGM. The presence of tree biomass at this time is also indicated by the results found here: Blocks 3, 6 and 7 contained a significantly ($p = 0.001$) lower amount of C_{25} than block 5. C_{25} has been shown to be enriched in woody root biomass compared to aboveground biomass (Gocke *et al.* 2014). The high amount of C_{25} in combination with C_{27}/C_{31} might imply that the contribution of wax alkanes by trees and shrubs at BL III was greatest at ∼26 ka. For 22.87 - 19.15 ka cal BP, the data of Magyari *et al.* indicated the persistence of forest with coniferous and deciduous trees at lower elevations as well as extreme continentality, which was reflected in increased fire activity. In the sedimentary record at BL III, evidence for such a rise in biomass burning could not be found. Expansion of vegetation adapted to extreme dryness (xerophytes) was reported straight after the onset of deglaciation 19.15 ka cal BP. Around 17 ka precipitation likely increased as the final melting of the Scandinavian Ice sheet led to a higher water discharge to the Black Sea and subsequently intensified vapour circulation in the Carpathians. At 16.3 ka cal BP, an advance in boreal woodland cover was demonstrated (Magyari *et al.* 2014).

4.5.3. Plant matter as fuel for fires

As summarized in Wolf *et al.* 2014, changing climatic conditions and with it the extent and composition of vegetation, most likely impacted fire activity, which was then preserved in the BC record of the Late Pleistocene. Fire severity, i.e. the peak temperature and fire duration (Certini 2005) is determined by the availability of fuel and the frequency of fires (Thevenon *et al.* 2010) and influences the amount of BC produced (Wolf *et al.* 2013). As discussed, the maximum temperatures achieved during fire depend on the material that is being burned. The fact that large quantities of BC were detected in soils under steppe vegetation and tropical rain forest but not in soils under savannas and boreal forests, even though fire frequency is usually greater in the latter, indicate that accumulation of BC in soils also depends on factors other than the amount of BC produced (Czimczik & Masiello 2007). Some of the BC can for example be lost in recurring fires (Czimczik & Masiello 2007). The quality of BC at BL III indicated low-temperature fires for all identified fire horizons. This supports what is implied by the alkane distribution patterns, i.e. that mainly grass vegetation was present at the time of all fires. It furthermore implies that the change in vegetation and/or climate, as implied by the shift in C_{27}/C_{31}, hardly affected the severity of the subsequent fires.

5. Limitations

This chapter focuses on the limitations that were encountered in the execution of the study. Limitations of the applied methods and analyses, e.g. the use of C_{27}/C_{31} as a molecular proxy for deriving palaeovegetation, were outlined in the discussion.

Taking samples

One limitation of this thesis was that taking samples from the blocks was based on visual distinction of seemingly interesting characteristics and changes of color within blocks. This may have led to unintentional omission of interesting (or an overestimation of uninteresting) features within blocks. On the same note, the delineation of fire horizons was not always clear, i.e. where they started or ended. As discussed, this was probably caused by mixing of the soil sediment, which led to similar but attenuated tendencies of the samples around fire horizons compared to fire horizons. The samples above and below fire horizons were therefore treated as separate sample groups.

Sample groups and size

These different sample types also posed a challenge when investigating the presence or absence of a depth dependent trend. In an attempt to account for this problem, fire horizons were excluded when comparing blocks. However, since samples above and below fire horizons often displayed the same but more subtle patterns, they too could possibly mask tendencies with depth. If they had been excluded as well, in many cases only two samples would have remained to represent a block. This would likely not produce any reliable results. Generally, small sample sizes for the different groups ($n = 4$ for fire horizons, samples above and below, $n = 3$ for rhizosphere) also limit the (statistical) power of the results and caution needs to be applied when drawing conclusions.

Cation exchange resin

As mentioned in the methods section, the cation exchange resin (BPCA method) had to be replaced. This was detected because the measured BPCA-C concentrations seemed quite low. As time constraints did not allow to repeat the analysis for all samples, the exact quantities that are reported in this thesis need to be taken with a grain of salt. Nevertheless, even if reported concentrations are systematically too low, this should not have affected the distribution pattern of BPCA-C, i.e. where concentrations are higher or lower. In order to obtain more accurate results on the actual quantities of BPCA-C, the whole analysis would have to be repeated.

6. Conclusion

Multi-methodological analyses of soil sediment samples from BL III supported the hypothesis that the four dark layers identified in the profile exhibited charring traces, i.e. were fire horizons. While the determination of the exact fire temperatures was not possible, it appeared that the fires in all horizons were not highly energetic. Likely, temperatures did not exceed 300 °C for the three fires in the upper part of the profile and were even lower in the oldest fire horizon. This suggests that plant biomass burning at low temperatures served as fuel, most likely grass vegetation. Plant wax lipid analyses supported the presumable predominance of grass vegetation at the time of the occurrence of all fires. They furthermore suggested a shift in the vegetation composition around the LGM. However, it is uncertain whether the changes in alkane chain length distribution were due to changes in vegetation or whether they were attributed to climatic changes, while the vegetation remained largely the same. The elemental composition of the soil and sediment material was generally similar throughout the whole profile. There was a difference in the abundance of certain elements in the fire horizons, especially TOC, N and Cu that were present in larger amounts. Si, V and Cr on the other hand, were depleted in the fire horizons, which might have been caused by leaching and subsequent accumulation in the layers below that had not been exposed to fire.

This study contributed to the ongoing research efforts in the Bistrița valley by providing insights about the palaeoenvironmental context of human habitation over the past ∼35 ka. Complimentary analyses such as pollen are however required to get a more reliable picture of the palaeovegetation at the site and in the broader region. To get a better understanding of the effects of biomass burning on the long-term elemental composition of soils, more studies about the fate of elements such as Cu, Zn, Fe and Mn (Certini 2005) are furthermore necessary.

References

1. Almendros, G., Martín, F. & González-Vila, F. J. Effects of fire on humic and lipid fractions in a Dystric Xerochrept in Spain. *Geoderma* **42,** 115–127 (1988).
2. Almendros, G., Knicker, H. & González-Vila, F. J. Rearrangement of carbon and nitrogen forms in peat after progressive thermal oxidation as determined by solid-state 13C- and 15N-NMR spectroscopy. *Organic Geochemistry* **34,** 1559–1568 (2003).
3. Anghelinu, M., Niţă, L. & Murătoreanu, G. Eastern Romanian Gravettian and Epigravettian: A reassessment. *Anthropologie (France)* **122,** 183–219 (2018).
4. Anghelinu, M., Niţâ, L., Sitlivy, V., Uthmeier, T. & Bâltean, I. Looking around Peştera Cu Oase: The beginnings of Upper Paleolithic in Romania. *Quaternary International* **274,** 136–157 (2012).
5. Angst, G., John, S., Mueller, C. W., Kögel-Knabner, I. & Rethemeyer, J. Tracing the sources and spatial distribution of organic carbon in subsoils using a multi-biomarker approach. *Scientific Reports* **6,** 1–12 (2016).
6. Bailey, A. W. & Anderson, M. L. Fire Temperatures in Forest Communities Grass, Shrub and Aspen of Central Alberta. *Journal of Range Management* **33,** 37–40 (1980).
7. Ballentine, D. C., MacKo, S. A. & Turekian, V. C. Variability of stable carbon isotopic compositions in individual fatty acids from combustion of C4 and C3 plants: Implications for biomass burning. *Chemical Geology* **152,** 151–161 (1998).
8. Banks, W. E., d'Errico, F., Peterson, A. T., Vanhaeren, M., Kageyama, M., Sepulchre, P., Ramstein, G., Jost, A. & Lunt, D. Human ecological niches and ranges during the LGM in Europe derived from an application of eco-cultural niche modeling. *Journal of Archaeological Science* **35,** 481–491 (2008).
9. Beyers, J. L., Brown, J. K., Busse, M. D., DeBano, L. F., Elliot, W. J., Ffolliott, P. F., Jacoby, G. R., Knoepp, J. D., Landsberg, J. D., Neary, D. G., Reardon, J. R., Rinne, J. N., Robichaud, P. R., Ryan, K. C., Tiedemann, A. R. & Zwolinski, M. J. *Wildland fire in ecosystems: effects of fire on soils and water* 2008th ed. (eds Neary, D. G., Ryan, K. C. & DeBano, L. F.) **42,** 250 (United States Department of Agriculture, Forest Service, Rocky Mountain Research Station, Ogden, 2005).
10. Bird, M. I., Moyo, C., Veenendaal, E. M., Lloyd, J. & Frost, P. Stability of elemental carbon in a savanna soil. *Global Biogeochemical Cycles* **13,** 923–932 (1999).
11. Bird, M. I. & Ascough, P. L. Isotopes in pyrogenic carbon: A review. *Organic Geochemistry* **42,** 1529–1539 (2012).
12. Budai, A., Calucci, L., Rasse, D. P., Strand, L. T., Pengerud, A., Wiedemeier, D., Abiven, S. & Forte, C. Effects of pyrolysis conditions on Miscanthus and corncob chars: Characterization by IR, solid state NMR and BPCA analysis. *Journal of Analytical and Applied Pyrolysis* **128,** 335–345 (2017).
13. Buggle, B., Wiesenberg, G. L. & Glaser, B. Is there a possibility to correct fossil n-alkane data for postsedimentary alteration effects? *Applied Geochemistry* **25,** 947–957 (2010).
14. Bush, R. T. & McInerney, F. A. Influence of temperature and C4 abundance on n-alkane chain length distributions across the central USA. *Organic Geochemistry* **79,** 65–73 (2015).

15. Bush, R. T. & McInerney, F. A. Leaf wax n-alkane distributions in and across modern plants: Implications for paleoecology and chemotaxonomy. *Geochimica et Cosmochimica Acta* **117,** 161–179 (2013).

16. Certini, G. Effects of fire on properties of forest soils: A review. *Oecologia* **143,** 1–10 (2005).

17. Chang, Z., Tian, L., Li, F., Zhou, Y., Wu, M., Steinberg, C. E., Dong, X., Pan, B. & Xing, B. Benzene polycarboxylic acid — A useful marker for condensed organic matter, but not for only pyrogenic black carbon. *Science of the Total Environment* **626,** 660–667 (2018).

18. Clark, P. U., Dyke, A. S., Shakun, J. D., Carlson, A. E., Clark, J., Wohlfarth, B., Mitrovica, J. X., Hostetler, S. W. & McCabe, A. M. The Last Glacial Maximum. *Science* **325,** 710–714 (2009).

19. Clausen, C. A. Bacterial associations with decaying wood: A review. *International Biodeterioration and Biodegradation* **37,** 101–107 (1996).

20. Cranwell, P. A. Diagenesis of free and bound lipids in terrestrial detritus deposited in a lacustrine sediment. *Organic Geochemistry* **3,** 79–89 (1981).

21. Czimczik, C. I. & Masiello, C. A. Controls on black carbon storage in soils. *Global Biogeochemical Cycles* **21,** 1–8 (2007).

22. Czimczik, C. I., Preston, C. M., Schmidt, M. W., Werner, R. A. & Schulze, E. D. Effects of charring on mass, organic carbon, and stable carbon isotope composition of wood. *Organic Geochemistry* **33,** 1207–1223 (2002).

23. Danu, M. & Bodi, G. Archaeological palynology in Romania? A review of its past and current state. *Studia Antiqua et Archaeologica* **21,** 113–121 (2015).

24. Darwin, C. *The Descent of Man, and Selection in Relation to Sex* 1st ed., 1–475 (Murray, John, London, 1871).

25. Dumitraşcu, V. & Vasile, Ş. Steppe bison hunting in the Gravettian of Buda (lower Bistriţa Valley, eastern Romania). *Anthropologie (France)* **122,** 166–182 (2018).

26. Eckmeier, E. & Wiesenberg, G. L. Short-chain n-alkanes (C16-20) in ancient soil are useful molecular markers for prehistoric biomass burning. *Journal of Archaeological Science* **36,** 1590–1596 (2009).

27. Eglinton, G., Gonzalez, A. G., Hamilton, R. J. & Raphael, R. A. Hydrocarbon constituents of the wax coatings of plant leaves: A taxonomic survey. *Phytochemistry* **1,** 89–102 (1962).

28. Eglinton, G. & Hamilton, R. J. Leaf epicuticular waxes. *Science* **156,** 1322–1335 (1967).

29. Gerke, J. Black (pyrogenic) carbon in soils and waters: a fragile data basis extensively interpreted. *Chemical and Biological Technologies in Agriculture* **6,** 1–8 (2019).

30. Glaser, B., Haumaier, L., Guggenberger, G. & Zech, W. Black carbon in soils: the use of benzenecarboxylic acids as specific markers. *Organic Geochemistry* **29,** 811–819 (1998).

31. Glaser, B. & Knorr, K. H. Isotopic evidence for condensed aromatics from non-pyrogenic sources in soils - Implications for current methods for quantifying soil black carbon. *Rapid Communications in Mass Spectrometry* **22,** 935–942 (2008).

32. Gocke, M., Kuzyakov, Y. & Wiesenberg, G. L. Rhizoliths in loess - evidence for post-sedimentary incorporation of root-derived organic matter in terrestrial sediments as assessed from molecular proxies. *Organic Geochemistry* **41,** 1198–1206 (2010).

33. Gocke, M., Kuzyakov, Y. & Wiesenberg, G. L. B. Differentiation of plant derived organic matter in soil, loess and rhizoliths based on n-alkane molecular proxies. *Biogeochemistry* **112,** 23–40 (2013).

34. Gocke, M., Peth, S. & Wiesenberg, G. L. Lateral and depth variation of loess organic matter overprint related to rhizoliths - Revealed by lipid molecular proxies and X-ray tomography. *Catena* **112,** 72–85 (2014).

35. González-Pérez, J. A., González-Vila, F. J., Almendros, G. & Knicker, H. The effect of fire on soil organic matter - A review. *Environment International* **30,** 855–870 (2004).

36. Jansen, B., Nierop, K. G., Hageman, J. A., Cleef, A. M. & Verstraten, J. M. The straight-chain lipid biomarker composition of plant species responsible for the dominant biomass production along two altitudinal transects in the Ecuadorian Andes. *Organic Geochemistry* **37,** 1514–1536 (2006).

37. Jansen, B. & Wiesenberg, G. L. Opportunities and limitations related to the application of plant-derived lipid molecular proxies in soil science. *SOIL* **3,** 211–234 (2017).

38. Knicker, H., Almendros, G., González-Vila, F. J., Martin, F. & Lüdemann, H. D. 13C- and 15N-NMR spectroscopic examination of the transformation of organic nitrogen in plant biomass during thermal treatment. *Soil Biology and Biochemistry* **28,** 1053–1060 (1996).

39. Kolattukudy, P., Croteau, R. & Buckner, J. *Biochemistry of Plant Waxes* in *Chemistry and Biochemistry of Natural Waxes* (ed Kolattukudy PE) 290–347 (Elsevier, Amsterdam, 1976).

40. Kuzyakov, Y., Subbotina, I., Chen, H., Bogomolova, I. & Xu, X. Black carbon decomposition and incorporation into soil microbial biomass estimated by 14C labeling. *Soil Biology and Biochemistry* **41,** 210–219 (2009).

41. Lei, G. L., Zhang, H. C., Chang, F. Q., Pu, Y., Zhu, Y., Yang, M. S. & Zhang, W. X. Biomarkers of modern plants and soils from Xinglong Mountain in the transitional area between the Tibetan and Loess Plateaus. *Quaternary International* **218,** 143–150 (2010).

42. López, S., van Dorp, L. & Hellenthal, G. Human dispersal out of Africa: A lasting debate. *Evolutionary Bioinformatics* **11,** 57–68 (2015).

43. Macadam, A. M. Effects of broadcast slash burning on fuels and soil chemical properties in the Sub-boreal Spruce Zone of central British Columbia. *Canadian Journal of Forest Research* **17,** 1577–1584 (1987).

44. Magyari, E., Veres, D., Wennrich, V., Wagner, B., Braun, M., Jakab, G., Karátson, D., Pál, Z., Ferenczy, G., St-Onge, G., Rethemeyer, J., Francois, J.-P., von Reumont, F. & Schäbitz, F. Vegetation and environmental responses to climate forcing during the Last Glacial Maximum and deglaciation in the East Carpathians: attenuated response to maximum cooling and increased biomass burning. *Quaternary Science Reviews* **106,** 278–298 (2014).

45. Mastrolonardo, G., Francioso, O., Di Foggia, M., Bonora, S., Rumpel, C. & Certini, G. Application of thermal and spectroscopic techniques to assess fire-induced changes to soil organic matter in a Mediterranean forest. *Journal of Geochemical Exploration* **143,** 174–182 (2014).

46. Moore, D. S., Notz, W. & Fligner, M. A. *The basic practice of statistics* 6th ed., 745 (W.H. Freeman & Company, a Macmillan Education Imprint, New York, 2013).

47. Mora, V., Baigorri, R., Bacaicoa, E., Zamarreño, A. M. & García-Mina, J. M. The humic acid-induced changes in the root concentration of nitric oxide, IAA and ethylene do not explain the changes in root architecture caused by humic acid in cucumber. *Environmental and Experimental Botany* **76,** 24–32 (2012).

48. Obreht, I., Zeeden, C., Hambach, U., Veres, D., Marković, S. B. & Lehmkuhl, F. A critical reevaluation of palaeoclimate proxy records from loess in the Carpathian Basin. *Earth-Science Reviews* **190,** 498–520 (2019).

49. Păunescu, A., Cârciumaru, E., Cârciumaru, M. & Vasilescu, P. Semnificaţia cronostratigrafică şi paleoclimatică a unor analize chimice, granulometrice şi palinologice în unele aşezări paleolitice din bazinul Ceahlăului. Consideraţii asupra tipului şi caracterului aşezărilor. *Studii şi Cercetări de Istorie Veche (şi Arheologie)* **28,** 157–184 (1977).

50. Ponomarenko, E., Tomson, P., Ershova, E. & Bakumenko, V. A multi-proxy analysis of sandy soils in historical slash-and-burn sites: A case study from southern Estonia. *Quaternary International* **516,** 190–206 (2019).

51. Sadori, L., Koutsodendris, A., Panagiotopoulos, K., Masi, A., Bertini, A., Combourieu-Nebout, N., Francke, A., Kouli, K., Joannin, S., Mercuri, A. M., Peyron, O., Torri, P., Wagner, B., Zanchetta, G., Sinopoli, G. & Donders, T. H. Pollen-based paleoenvironmental and paleoclimatic change at Lake Ohrid (south-eastern Europe) during the past 500 ka. *Biogeosciences* **13,** 1423–1437 (2016).

52. Schäfer, I. K., Bliedtner, M., Wolf, D., Faust, D. & Zech, R. Evidence for humid conditions during the last glacial from leaf wax patterns in the loess-paleosol sequence El Paraíso, Central Spain. *Quaternary International* **407,** 64–73 (2016).

53. Schmidt, C., Anghelinu, M., Hambach, U., Veres, D. & Lehmkuhl, F. Reassessing the timeframe of Upper Palaeolithic deposits in the Ceahlău Basin (Eastern Carpathians, Romania): Geochronological and archaeological implications. *Quaternary Geochronology* **55,** 101020 (2020).

54. Schmidt, M. W. I., Skjemstad, J. O., Gehrt, E. & Kogel-Knabner, I. Charred organic carbon in German chernozemic soils. *European Journal of Soil Science* **50,** 351–365 (1999).

55. Schmidt, M. W. & Noack, A. G. Black carbon in soils and sediments: Analysis, distribution, implications, and current challenges. *Global Biogeochemical Cycles* **14,** 777–793 (2000).

56. Schneider, M. P., Hilf, M., Vogt, U. F. & Schmidt, M. W. The benzene polycarboxylic acid (BPCA) pattern of wood pyrolyzed between 200 °C and 1000 °C. *Organic Geochemistry* **41,** 1082–1088 (2010).

57. Schwark, L., Zink, K. & Lechterbeck, J. Reconstruction of postglacial to early Holocene vegetation history in terrestrial Central Europe via cuticular lipid biomarkers and pollen records from lake sediments. *Geology* **30,** 463–466 (2002).

58. Simpson, M. J. & Hatcher, P. G. Overestimates of black carbon in soils and sediments. *Naturwissenschaften* **91,** 436–440 (2004).

59. Smith, D. W. Concentrations of soil nutrients before and after fire. *Canadian Journal of Soil Science* **50,** 17–29 (1970).

60. Stankov Jovanovic, V. P., Ilic, M. D., Markovic, M. S., Mitic, V. D., Nikolic Mandic, S. D. & Stojanovic, G. S. Wild fire impact on copper, zinc, lead and cadmium distribution in soil and relation with abundance in selected plants of Lamiaceae family from Vidlic Mountain (Serbia). *Chemosphere* **84,** 1584–1591 (2011).

61. Steguweit, L., Cârciumaru, M., Anghelinu, M. & Niţă, L. Reframing the Upper Palaeolithic in the Bistriţa Valley (northeastern Romania). *Quartär* **56,** 139–157 (2009).

62. Stevenson, F. J. *Humus Chemistry* (Wiley, New York, 1982).

63. Stinson, K. J. & Wright, H. A. Temperatures of Headfires in the Southern Mixed Prairie of Texas. *Journal of Range Management* **22,** 169 (1969).

64. Thevenon, F., Williamson, D., Bard, E., Anselmetti, F. S., Beaufort, L. & Cachier, H. Combining charcoal and elemental black carbon analysis in sedimentary archives: Implications for past fire regimes, the pyrogenic carbon cycle, and the human–climate interactions. *Global and Planetary Change* **72,** 381–389 (2010).

65. Tomescu, A. M. F. Evaluation of Holocene pollen records from the Romanian Plain. *Review of Palaeobotany and Palynology* **109,** 219–233 (2000).

66. Trandafir, O., Timar-Gabor, A., Schmidt, C., Veres, D., Anghelinu, M., Hambach, U. & Simon, S. OSL dating of fine and coarse quartz from a Palaeolithic sequence on the Bistrita Valley (Northeastern Romania). *Quaternary Geochronology* **30,** 487–492 (2015).

67. Trinkaus, E., Moldovan, O., Milota, Ş., Bîlgăr, A., Sarcina, L., Athreya, S., Bailey, S. E., Rodrigo, R., Mircea, G., Higham, T., Bronk Ramsey, C. & Van der Plicht, J. An early modern human from the Peştera cu Oase, Romania. *Proceedings of the National Academy of Sciences of the United States of America* **100,** 11231–11236 (2003).

68. Turekian, V. C., MacKo, S., Ballentine, D., Swap, R. J. & Garstang, M. Causes of bulk carbon and nitrogen isotopic fractionations in the products of vegetation burns: Laboratory studies. *Chemical Geology* **152,** 181–192 (1998).

69. Turney, C. S., Wheeler, D. & Chivas, A. R. Carbon isotope fractionation in wood during carbonization. *Geochimica et Cosmochimica Acta* **70,** 960–964 (2006).

70. Ulery, A. L. & Graham, R. C. Forest Fire Effects on Soil Color and Texture. *Soil Science Society of America Journal* **57,** 135–140 (1993).

71. Underhill, P. A. & Kivisild, T. Use of Y Chromosome and Mitochondrial DNA Population Structure in Tracing Human Migrations. *Annual Review of Genetics* **41,** 539–564 (2007).

72. Wiedemeier, D. B., Brodowski, S. & Wiesenberg, G. L. Pyrogenic molecular markers: Linking PAH with BPCA analysis. *Chemosphere* **119,** 432–437 (2015).

73. Wiedemeier, D. B., Hilf, M. D., Smittenberg, R. H., Haberle, S. G. & Schmidt, M. W. Improved assessment of pyrogenic carbon quantity and quality in environmental samples by high-performance liquid chromatography. *Journal of Chromatography A* **1304,** 246–250 (2013).

74. Wiedemeier, D. B., Lang, S. Q., Gierga, M., Abiven, S., Bernasconi, S. M., Früh-Green, G. L., Hajdas, I., Hanke, U. M., Hilf, M. D., McIntyre, C. P., Scheider, M. P. W., Smittenberg, R. H., Wacker, L., Wiesenberg, G. L. B. & Schmidt, M. W. I. Characterization, Quantification and Compound-specific Isotopic Analysis of Pyrogenic Carbon Using Benzene Polycarboxylic Acids (BPCA). *Journal of Visualized Experiments* (2016).

75. Wiesenberg, G. L., Lehndorff, E. & Schwark, L. Thermal degradation of rye and maize straw: Lipid pattern changes as a function of temperature. *Organic Geochemistry* **40,** 167–174 (2009).

76. Wiesenberg, G. L. B. & Gocke, M. I. *Analysis of Lipids and Polycyclic Aromatic Hydrocarbons as Indicators of Past and Present (Micro)Biological Activity* in, 61–91 (Springer, Berlin, Heidelberg, 2015).

77. Wolf, M., Lehndorff, E., Mrowald, M., Eckmeier, E., Kehl, M., Frechen, M., Pätzold, S. & Amelung, W. Black carbon: Fire fingerprints in Pleistocene loess-palaeosol archives in Germany. *Organic Geochemistry* **70,** 44–52 (2014).

78. Wolf, M., Lehndorff, E., Wiesenberg, G. L., Stockhausen, M., Schwark, L. & Amelung, W. Towards reconstruction of past fire regimes from geochemical analysis of charcoal. *Organic Geochemistry* **55,** 11–21 (2013).

79. Zech, M., Buggle, B., Leiber, K., Marković, S., Glaser, B., Hambach, U., Huwe, B., Stevens, T., Sümegi, P., Wiesenberg, G. & Zöller, L. Reconstructing Quaternary vegetation history in the Carpathian Basin, SE Europe, using n-alkane biomarkers as molecular fossils. *E&G* **58,** 148–155 (2009).

Appendix A Supplementary data

sample	block	depth [cm]	description	sample weight [g]	stone weight [g]	total weight [g]
213B19DB1	7		top right (front view)	183.78	0	183.78
213B19DB2	7		rhizosphere	41.88	0	41.88
213B19DB2A	7	64	roots	0.12	0	0.12
213B19DB3	7		middle (front views)	114.18	0	114.18
213B19DB4	7		bottom left above reddish area (front view)	126.08	0	126.08
213B19DB5	7		reddish area, bottom left (front view)	90.08	0	90.08
213B19DB6	6		digging passages from the front side (top right and middle -> connected)	56.78	0	56.78
213B19DB7	6		clearly above from carbon layer (top from the left side)	123.98	0.1	124.08
213B19DB8	6		just above carbon layer	127.68	0	127.68
213B19DB9	6		carbon layer	155.38	0.1	155.48
213B19DB10	6	105	just below carbon layer	109.28	0	109.28
213B19DB11	6		rhizosphere	35.38	1	36.38
213B19DB11A	6		roots	0.12	0	0.12
213B19DB12	6		clearly below carbon layer (bottom from the left side)	134.38	0	134.38
213B19DB13	6		tools/artifacts	9.18	0	9.18
213B19DB14	5		rhizosphere	70.08	0	70.08
213B19DB14A	5		roots	0.02	0	0.02
213B19DB15	5		whitish area with brown edge from the top side (snail?)	64.68	0	64.68
213B19DB16	5	135	clearly above carbon layer, left side	111.08	0	111.08
213B19DB17	5		slightly above carbon layer, front and left side	105.68	0	105.68
213B19DB18	5		carbon layer, right, left & front side	90.08	0	90.08
213B19DB19	5		slightly below carbon layer, left, right, front side	111.78	0	111.78
213B19DB20	5		clearly below carbon layer, left side	116.78	0	116.78
213B19DB21	4		charcoal piece and a small amount of bulk material	4.18	0	4.18
213B19DB22	4		top left corner (front), whitish/lighter colored	88.28	0	88.28
213B19DB23	4		diagonally below (front: top right corner to left side)	88.78	0	88.78
213B19DB24	4	170	diagonally below (front: right side to left side, where xx23 ended)	92.58	0	92.58
213B19DB24A	4		roots	0.02	0	0.02
213B19DB25	4		straight below 213B19DB24	83.98	0	83.98
213B19DB26	4		bottom of the front side; I cut off ca. 2 cm from the front	109.28	0	109.28
213B19DB27	3		wood (from the front and top side)	13.38	0	13.38
213B19DB28	3		red minerals (tiny), taken from throughout the block	0.68	0	0.68
213B19DB29	3		blade; very small, white hard pieces from the left, top and a bigger one from the top)	4.98	0	4.98
213B19DB30	3	185	block from the left side (top right corner) that was falling out	25.58	0	25.58
213B19DB31	3		top of front side; above area with more carbon	105.18	0	105.18
213B19DB32	3		area with more carbon; front side	106.18	0	106.18
213B19DB33	3		area where the wood was recovered from; front side	94.98	0.1	95.08
213B19DB34	3		bottom left (front side); below the wood	107.38	0	107.38
213B19DB35	2		above brown layer	94.78	0	94.78
213B19DB36	2		within brown layer but above carbon/darker area	91.18	0	91.18
213B19DB37	2	200	carbon/darker part of the brown layer	128.08	0	128.08
213B19DB38	2		just below the layer	102.78	0	102.78
213B19DB39	2		clearly below the layer	152.38	0	152.38
213B19DB40	1		part that seems darker	218.28	1.8	220.08
213B19DB41	1		below darker part	308.68	3.8	312.48
213B19DB42	1	237	above lighter part	307.78	1.9	309.68
213B19DB43	1		slightly lighter part	253.68	1.1	254.78
213B19DB44	1		roots	0.02	0	0.02
213B19DB45			combination of all root samples	0.1	0	0.1

sample	Na	Mg	Al	Si	P	S	Cl	K	Ca	Ti	Mn	Fe	C	N	δ13C
	[%]	[%]	[%]	[%]	[%]	[%]	[%]	[%]	[%]	[%]	[%]	[%]	[mg g^-1]	[mg g^-1]	[‰ V-PDB]
213B19BD1	1.322	1.547	9.350	27.52	0.05871	0.03303	0.00344	2.810	0.3254	0.5741	0.08667	4.675	2.579	0.342	-25.602
213B19DB2	1.410	1.454	8.891	26.94	0.05805	0.03282	0.0049	2.722	0.3094	0.5765	0.07881	4.487	2.303	0.337	-26.101
213B19DB3	1.448	1.536	9.083	27.34	0.06170	0.03259	0.003	2.791	0.3000	0.5661	0.08076	4.561	2.305	0.316	-26.173
213B19DB4	1.381	1.504	9.102	27.20	0.06363	0.03334	0.00344	2.861	0.3092	0.5792	0.08045	4.569	2.363	0.349	-26.172
213B19DB5	1.314	1.501	9.057	27.11	0.07356	0.03277	0.00311	2.822	0.3020	0.5812	0.0722	4.544	2.182	0.321	-26.283
213B19DB6	1.358	1.517	8.914	27.24	0.14440	0.03327	0.00422	2.802	0.3923	0.5550	0.08597	4.526	3.106	0.317	-25.465
213B19DB7	1.405	1.548	9.154	27.35	0.13730	0.03384	0.00543	2.798	0.4179	0.5645	0.09028	4.628	2.881	0.330	-25.546
213B19BD8	1.453	1.509	9.146	27.40	0.15550	0.03241	0.00337	2.805	0.4303	0.5752	0.09402	4.525	3.413	0.361	-25.189
213B19BD9	1.401	1.492	8.911	26.90	0.30400	0.03399	0.00347	2.740	0.6044	0.5699	0.09373	4.591	7.433	0.415	-24.327
213B19DB10	1.400	1.457	8.861	27.00	0.14710	0.03038	0.00339	2.756	0.4074	0.5483	0.0831	4.537	2.640	0.326	-25.525
213B19DB11	1.393	1.457	8.900	27.12	0.24050	0.03267	0.00411	2.741	0.5031	0.5700	0.09027	4.600	4.762	0.418	-25.097
213B19DB12	1.415	1.522	9.023	27.73	0.13850	0.03102	0.00473	2.801	0.3964	0.5782	0.0812	4.498	2.652	0.302	-25.779
213B19DB14	1.443	1.458	8.744	26.96	0.09600	0.03284	0.00602	2.775	0.4030	0.5788	0.08499	4.482	2.299	0.321	-25.832
213B19DB15	1.493	1.487	8.893	27.49	0.10160	0.03262	0.00398	2.801	0.3963	0.5658	0.07835	4.374	2.050	0.273	-25.985
213B19DB16	1.385	1.495	8.989	27.44	0.09660	0.03139	0.00339	2.819	0.4159	0.5696	0.08756	4.525	2.197	0.304	-25.907
213B19BD17	1.348	1.486	8.942	27.51	0.08469	0.03211	0.00329	2.761	0.3950	0.5674	0.08513	4.494	2.297	0.298	-25.666
213B19DB18	1.304	1.487	8.793	27.02	0.10000	0.03163	0.00379	2.706	0.4274	0.5820	0.09036	4.544	4.840	0.420	-24.344
213B19DB19	1.392	1.503	8.993	27.02	0.07988	0.03077	0.00386	2.785	0.4008	0.5656	0.08838	4.429	2.626	0.322	-25.338
213B19DB20	1.411	1.508	9.068	27.62	0.07820	0.03297	0.00369	2.823	0.4108	0.5629	0.08262	4.447	1.888	0.281	-26.138
213B19DB21	-	-	-	-	-	-	-	-	-	-	-	-	10.711	0.343	-23.566
213B19DB22	1.545	1.525	8.825	27.06	0.08467	0.03631	0.00395	2.811	0.3968	0.5781	0.08817	4.399	2.275	0.304	-25.795
213B19DB23	1.331	1.457	8.680	27.25	0.08388	0.03624	0.0044	2.828	0.4015	0.5835	0.08815	4.431	2.191	0.287	-25.888
213B19DB24	1.454	1.508	8.909	27.41	0.08900	0.03554	0.00474	2.837	0.4053	0.5732	0.08633	4.349	2.270	0.287	-26.054
213B19DB25	1.499	1.519	9.022	28.00	0.10610	0.03801	0.00352	2.847	0.4225	0.5901	0.1019	4.404	2.526	0.311	-25.388
213B19BD26	1.400	1.489	8.884	27.61	0.10380	0.03853	0.00971	2.825	0.4325	0.5702	0.08655	4.450	2.479	0.302	-25.347
213B19DB27	1.606	1.298	7.355	17.72	7.89400	0.05041	< 0.00020	1.945	12.8000	0.4419	0.3408	6.173	-	-	-
213B19DB28	-	-	-	-	-	-	-	-	-	-	-	-	5.565	0.367	-24.483
213B19DB30	1.449	1.440	8.719	27.43	0.14070	0.03337	0.0041	2.770	0.4856	0.5713	0.08758	4.308	2.893	0.302	-25.078
213B19DB31	1.412	1.464	8.810	27.40	0.15880	0.03544	0.00337	2.788	0.4973	0.5753	0.08672	4.441	9.464	0.388	-24.267
213B19DB32	1.326	1.465	8.837	26.90	0.21300	0.03545	0.00432	2.736	0.6045	0.5753	0.08378	4.451	6.718	0.372	-23.647
213B19DB33	1.363	1.506	8.945	27.75	0.31030	0.03622	0.00452	2.770	0.7134	0.5596	0.08136	4.410	3.976	0.339	-24.038
213B19DB34	1.698	1.699	10.140	31.69	0.16420	0.03824	0.00392	3.194	0.5516	0.6557	0.09562	5.063	2.240	0.285	-25.406
213B19BD35	1.395	1.450	8.832	27.06	0.05229	0.03552	0.0032	2.840	0.4080	0.5667	0.087	4.357	2.392	0.343	-25.335
213B19DB36	1.380	1.546	9.133	27.36	0.04942	0.03335	0.00389	2.921	0.4151	0.5808	0.08316	4.407	3.113	0.466	-25.465
213B19DB37	1.416	1.527	9.061	27.26	0.04995	0.03272	0.0042	2.849	0.4523	0.5800	0.08628	4.480	6.502	0.823	-24.436
213B19DB38	1.457	1.497	8.954	27.02	0.04725	0.03326	0.00217	2.818	0.4125	0.5655	0.09011	4.449	2.459	0.370	-25.823
213B19DB39	1.409	1.476	9.009	27.45	0.04857	0.0339	0.00177	2.751	0.4124	0.5830	0.09476	4.312	2.253	0.318	-25.851
213B19DB40	1.203	1.361	8.778	27.00	0.06579	0.0377	0.00239	2.389	0.4380	0.5637	0.1055	4.196	2.690	0.349	-25.424
213B19DB41	1.269	1.348	8.890	26.91	0.06715	0.03942	< 0.00020	2.580	0.4457	0.5695	0.08788	4.335	2.912	0.401	-25.276
213B19DB42	1.303	1.426	9.058	27.18	0.06482	0.04109	0.00311	2.678	0.4471	0.5506	0.07979	4.339	2.837	0.422	-25.209
213B19DB43	1.372	1.400	8.937	26.91	0.07124	0.03951	0.00186	2.635	0.4467	0.5645	0.07453	4.290	2.644	0.396	-25.445

sample	Total free extractable lipid content			BPCA-C	B3CA	B4CA	B5CA	B6CA
	extracted weight [µg]	µg g^-1 sample	mg ^-1 TOC	[g kg^-1 TOC]	[% of total BPCA]	[% of total BPCA]	[% of total BPCA]	[% of total BPCA]
213B19DB1	700	40	15	15	5	21	38	36
213B19DB2	1230	66	29	18	5	23	40	32
213B19DB3	710	37	16	43	4	19	38	40
213B19DB4	420	23	10	16	5	21	38	37
213B19DB5	700	42	19	13	5	23	41	30
213B19DB6	1570	91	29	40	7	28	38	27
213B19DB7	680	43	15	34	6	26	39	29
213B19DB8	670	45	13	55	6	26	37	32
213B19DB9	1810	52	7	99	6	29	34	31
213B19DB10	2210	61	23	30	5	24	36	34
213B19DB11	1890	118	25	72	7	27	37	29
213B19DB12	1590	48	18	14	6	27	41	26
213B19DB14	1520	93	40	42	7	30	39	24
213B19DB15	1120	70	34	20	6	26	40	28
213B19DB16	200	11	5	21	7	27	41	26
213B19DB17	440	26	11	37	7	28	41	24
213B19DB18	850	49	10	110	7	31	36	26
213B19DB19	740	49	19	39	9	31	42	18
213B19DB20	790	44	23	19	9	32	45	14
213B19DB21	-	-	-	183	9	40	30	21
213B19DB22	830	50	22	27	5	25	38	32
213B19DB23	710	51	23	19	7	32	48	13
213B19DB24	700	44	19	23	6	28	44	21
213B19DB25	1000	54	21	21	7	31	47	16
213B19DB26	680	41	16	32	6	29	40	25
213B19DB30	1830	117	40	52	4	21	42	34
213B19DB31	1070	63	7	35	6	25	36	33
213B19DB32	600	38	6	102	4	26	33	36
213B19DB33	720	53	13	91	7	29	35	29
213B19DB34	970	62	28	28	7	26	36	30
213B19DB35	1100	67	28	30	7	26	38	29
213B19DB36	550	40	13	21	12	35	41	11
213B19DB37	940	55	9	47	12	34	41	13
213B19DB38	460	25	10	28	7	27	38	28
213B19DB39	870	49	22	22	5	23	37	34
213B19DB40	950	48	18	24	8	32	42	18
213B19DB41	520	25	9	20	7	29	42	23
213B19DB42	640	35	12	18	6	28	41	25
213B19DB43	730	36	14	22	5	24	37	33

sample	normalized alkane amounts [µg g^-1 TOC]																		normalized amount [µg g^-1 TOC]	
	C16	C17	C18	C19	C20	C21	C22	C23	C24	C25	C26	C27	C28	C29	C30	C31	C32	C33	pristane	phytane
213B19DB1	8	16	23	11	12	5	5	4	4	3	2	4	1	13	1	10	3	3	5	9
213B19DB2	7	18	28	13	18	7	7	5	6	3	3	5	2	19	3	16	5	5	3	9
213B19DB3	3	10	19	11	14	6	6	5	4	3	3	6	1	22	3	19	4	5	3	7
213B19DB4	6	13	19	10	11	5	5	5	4	4	3	6	2	17	2	15	4	5	5	6
213B19DB5	5	15	24	13	14	7	6	5	5	3	3	5	2	19	3	16	6	5	5	8
213B19DB6	6	14	18	8	13	5	5	5	5	5	4	3	3	22	4	19	7	6	5	8
213B19DB7	2	11	17	11	11	8	7	7	5	5	4	7	2	20	4	18	5	5	3	7
213B19DB8	2	10	15	9	9	6	6	6	3	5	3	7	2	17	2	15	3	4	3	5
213B19DB9	3	8	8	4	4	2	2	2	1	2	1	3	1	8	1	8	1	2	1	2
213B19DB10	6	12	18	10	13	7	7	8	5	6	4	8	2	26	3	24	5	6	2	5
213B19DB11	2	14	25	15	12	7	7	5	4	3	3	4	2	16	2	13	5	5	4	7
213B19DB12	3	11	19	9	13	6	6	7	4	6	3	9	2	25	3	23	5	6	2	7
213B19DB14	3	24	38	21	19	11	2	10	8	8	6	14	4	42	6	37	7	10	5	13
213B19DB15	4	15	24	13	16	9	9	10	5	10	6	18	3	46	5	37	6	9	6	9
213B19DB16	4	14	21	13	15	10	12	11	8	10	7	16	4	51	6	37	11	12	3	8
213B19DB17	6	14	18	10	12	6	7	8	4	8	5	16	1	44	3	34	4	8	11	9
213B19DB18	1	5	8	4	6	3	2	2	2	2	2	4	1	13	1	12	2	3	2	4
213B19DB19	2	9	16	10	13	7	7	8	5	8	5	15	1	43	4	43	4	12	3	7
213B19DB20	1	5	16	9	16	6	7	12	4	11	5	20	2	50	6	64	4	15	9	7
213B19DB22	9	23	24	12	16	7	7	10	5	12	4	18	2	46	6	60	6	14	5	12
213B19DB23	1	6	14	9	16	5	6	7	5	5	4	8	2	28	5	33	5	9	2	4
213B19DB24	2	8	15	8	16	6	6	9	6	7	5	14	3	45	6	56	6	12	3	4
213B19DB25	6	11	15	8	12	4	5	6	5	5	4	8	2	30	5	35	6	8	4	4
213B19DB26	7	12	13	7	10	5	4	6	3	6	3	12	1	42	5	58	3	12	3	6
213B19DB30	7	16	22	13	25	6	8	6	8	5	6	7	5	40	7	48	12	15	5	10
213B19DB31	1	3	5	3	4	2	2	2	1	2	1	3	1	11	2	16	1	4	0	2
213B19DB32	0	2	4	2	5	2	2	2	2	2	1	4	0	14	2	19	2	5	1	2
213B19DB33	6	10	11	5	8	3	3	3	3	3	2	6	1	21	3	28	2	7	2	5
213B19DB34	9	22	25	13	18	9	8	8	5	8	5	13	2	40	6	42	6	11	17	15
213B19DB35	4	9	8	4	6	3	3	5	2	5	3	10	1	25	3	29	2	7	3	3
213B19DB36	7	12	15	7	11	4	4	3	3	4	3	7	1	22	3	24	4	7	2	5
213B19DB37	4	7	8	4	6	2	2	1	2	1	1	3	1	10	1	13	2	4	2	2
213B19DB38	1	3	8	5	13	4	5	5	5	7	5	14	3	48	6	65	6	18	1	2
213B19DB39	9	15	16	8	13	5	6	8	5	11	6	23	2	70	8	103	5	26	4	4
213B19DB40	2	5	9	5	7	4	4	5	2	5	3	10	1	28	4	35	2	14	1	3
213B19DB41	4	10	10	4	5	3	3	5	1	6	3	11	0	31	3	43	1	13	2	4
213B19DB42	4	10	9	4	4	3	3	6	1	7	3	10	0	29	3	39	1	11	1	4
213B19DB43	4	16	18	9	8	6	6	8	2	7	3	12	0	32	3	42	2	13	7	6

sample	normalized alkane amounts [ng g^-1]																		normalized amount [ng g^-1]	
	C16	C17	C18	C19	C20	C21	C22	C23	C24	C25	C26	C27	C28	C29	C30	C31	C32	C33	pristane	phytane
213B19DB1	22	42	60	27	31	13	12	10	9	8	5	11	2	33	4	26	7	7	14	23
213B19DB2	17	41	64	30	42	15	15	12	14	8	8	12	6	44	6	38	12	12	7	20
213B19DB3	7	24	43	25	32	14	13	11	9	8	7	15	3	51	6	43	8	12	7	15
213B19DB4	15	32	45	23	27	13	11	11	9	9	7	14	4	40	5	36	8	11	11	13
213B19DB5	12	32	53	27	30	15	14	11	12	6	7	10	5	41	7	35	12	11	11	18
213B19DB6	20	44	56	24	42	15	16	15	16	15	12	11	9	67	13	60	23	19	17	25
213B19DB7	5	32	49	31	31	22	21	21	14	16	11	19	6	58	11	53	15	15	9	19
213B19DB8	7	34	52	30	30	21	19	22	12	17	10	22	5	59	7	51	10	14	9	16
213B19DB9	21	57	60	28	32	17	16	18	10	15	9	22	4	59	6	56	11	13	7	15
213B19DB10	16	32	47	26	33	18	18	21	12	15	10	22	6	68	9	63	13	17	5	13
213B19DB11	12	65	119	70	59	35	34	25	21	16	15	18	10	77	10	64	22	22	17	35
213B19DB12	7	29	52	25	34	15	15	17	10	16	9	24	5	66	9	61	13	17	5	18
213B19DB14	7	55	88	48	44	26	6	24	18	19	13	31	8	96	14	85	15	24	12	31
213B19DB15	8	30	49	27	33	18	17	21	11	20	12	37	6	95	10	76	13	18	12	18
213B19DB16	9	31	47	30	32	22	26	25	17	22	15	34	8	113	13	82	25	26	6	18
213B19DB17	13	32	41	22	28	15	16	19	10	19	11	36	3	101	8	79	10	8	25	21
213B19DB18	6	26	40	21	28	14	12	12	8	11	7	22	4	62	5	58	8	15	8	18
213B19DB19	6	23	41	25	33	17	17	22	13	20	12	40	4	113	11	114	10	31	8	18
213B19DB20	1	9	30	17	30	12	13	23	8	21	9	37	4	94	11	120	8	28	16	13
213B19DB22	20	52	56	28	37	15	15	24	11	28	10	41	5	104	13	137	13	32	10	27
213B19DB23	2	13	30	19	36	10	13	14	10	10	9	16	5	62	11	73	11	20	5	9
213B19DB24	5	18	33	19	37	13	14	20	13	16	11	31	6	102	14	126	14	32	6	9
213B19DB25	15	28	38	21	31	11	13	15	12	13	10	20	6	76	12	88	14	21	9	11
213B19DB26	18	30	33	17	25	12	10	15	9	15	8	30	3	104	11	144	8	29	8	14
213B19DB30	20	47	65	38	73	18	23	17	24	15	17	20	13	116	21	138	34	42	14	28
213B19DB31	6	29	47	27	36	20	19	19	13	18	12	28	6	106	18	150	13	39	4	20
213B19DB32	1	11	29	15	34	13	13	15	11	15	10	27	3	93	12	129	11	32	7	11
213B19DB33	22	39	45	20	33	12	13	13	10	14	10	24	5	84	12	112	10	28	7	19
213B19DB34	20	49	56	30	39	19	18	18	12	18	11	29	4	89	12	93	14	25	37	33
213B19DB35	10	21	20	11	15	8	8	11	5	13	7	24	3	60	8	68	6	17	8	8
213B19DB36	21	36	47	21	35	11	13	10	10	12	10	21	4	70	9	76	12	22	6	14
213B19DB37	28	46	55	23	37	13	12	9	12	9	9	17	4	63	9	83	12	23	10	15
213B19DB38	1	8	21	13	31	10	13	12	13	17	13	35	7	118	15	159	14	43	3	6
213B19DB39	20	33	37	19	29	12	14	18	11	24	14	52	4	159	18	233	11	55	9	10
213B19DB40	4	14	24	14	19	10	10	14	5	14	8	26	2	74	11	95	6	28	2	9
213B19DB41	12	28	28	13	15	9	9	16	4	17	8	31	1	89	9	125	4	38	5	13
213B19DB42	11	27	26	12	11	10	10	17	3	19	7	29	1	82	8	111	2	28	4	10
213B19DB43	11	41	47	23	22	15	15	20	6	19	9	31	1	85	8	111	5	34	18	17

Appendix B Pictures from sampling at BLIII

Figure B.23: Pictures from the sampling at BLIII in the summer of 2018 (all pictures: U. Hambach)

Appendix C Results

C.1 Elemental composition

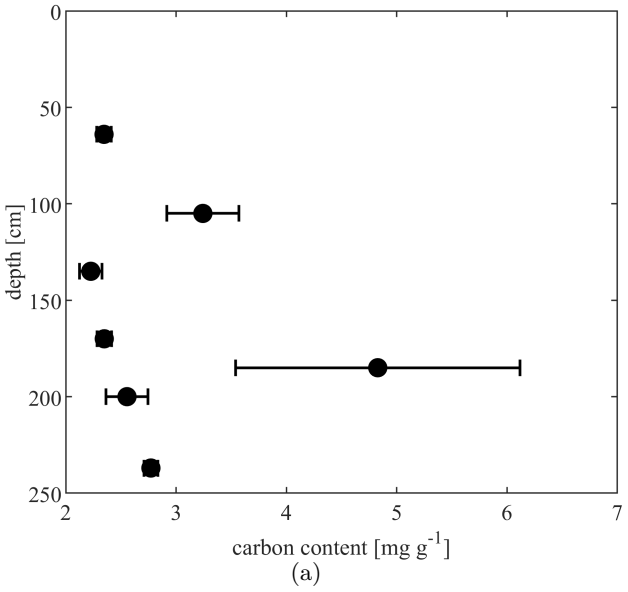

(a)

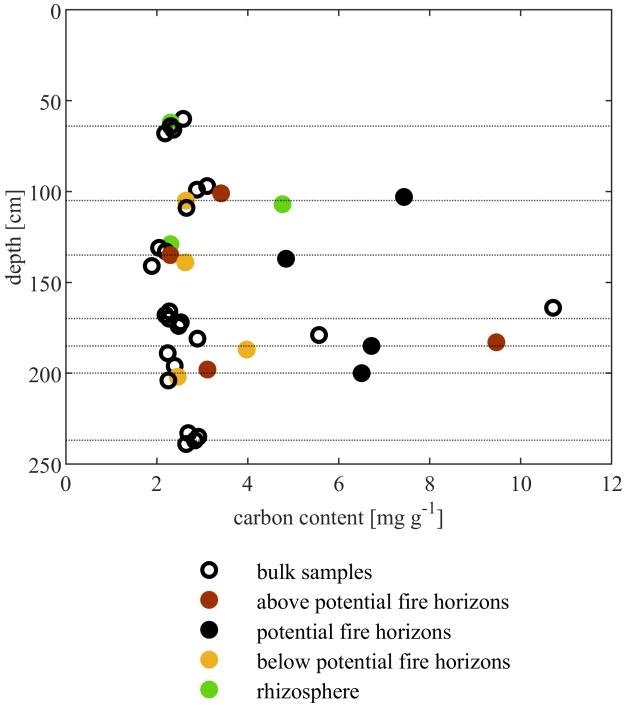

(b)

Figure C.24: The average carbon contents per sample weight for each block (a). Error bars represent the standard error of the mean. Picture (b) shows the carbon contents for all samples.

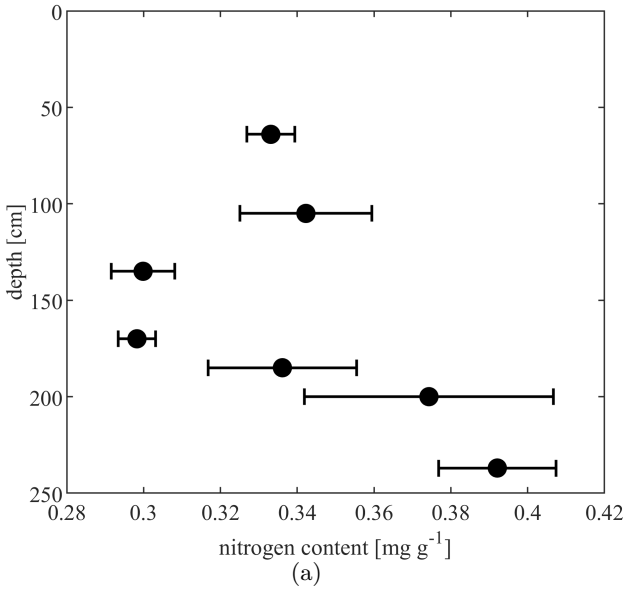

(a)

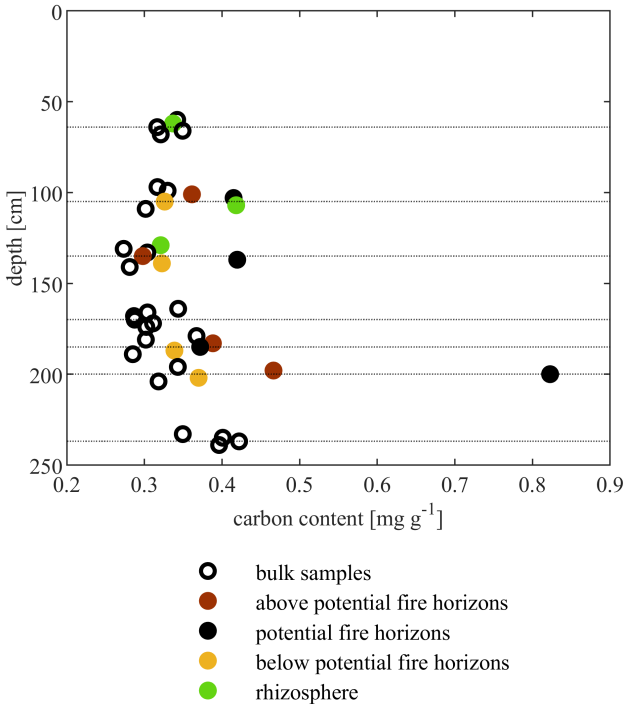

(b)

Figure C.25: The average nitrogen contents per sample weight for each block (a). Error bars represent the standard error of the mean. Picture (b) shows the nitrogen contents for all samples.

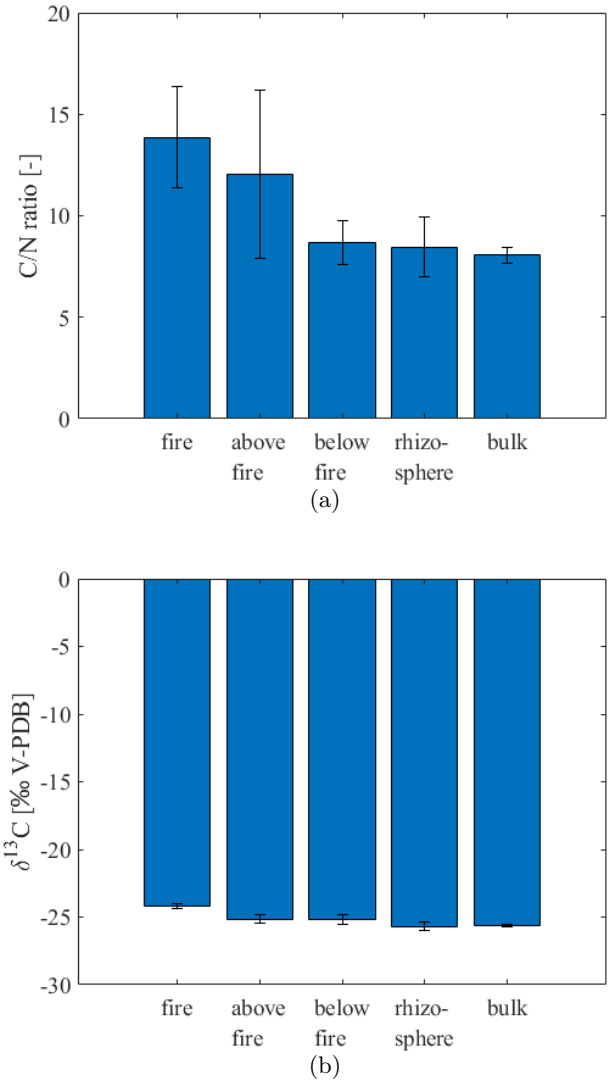

Figure C.26: The C/N ratio (a) and the isotopic signature (b) for the sample groups. The C/N ratio did not differ significantly between sample groups. The average δ^{13}C for fire samples differed significantly from the isotopic signature of all other groups. Bars represent the standard error of the mean.

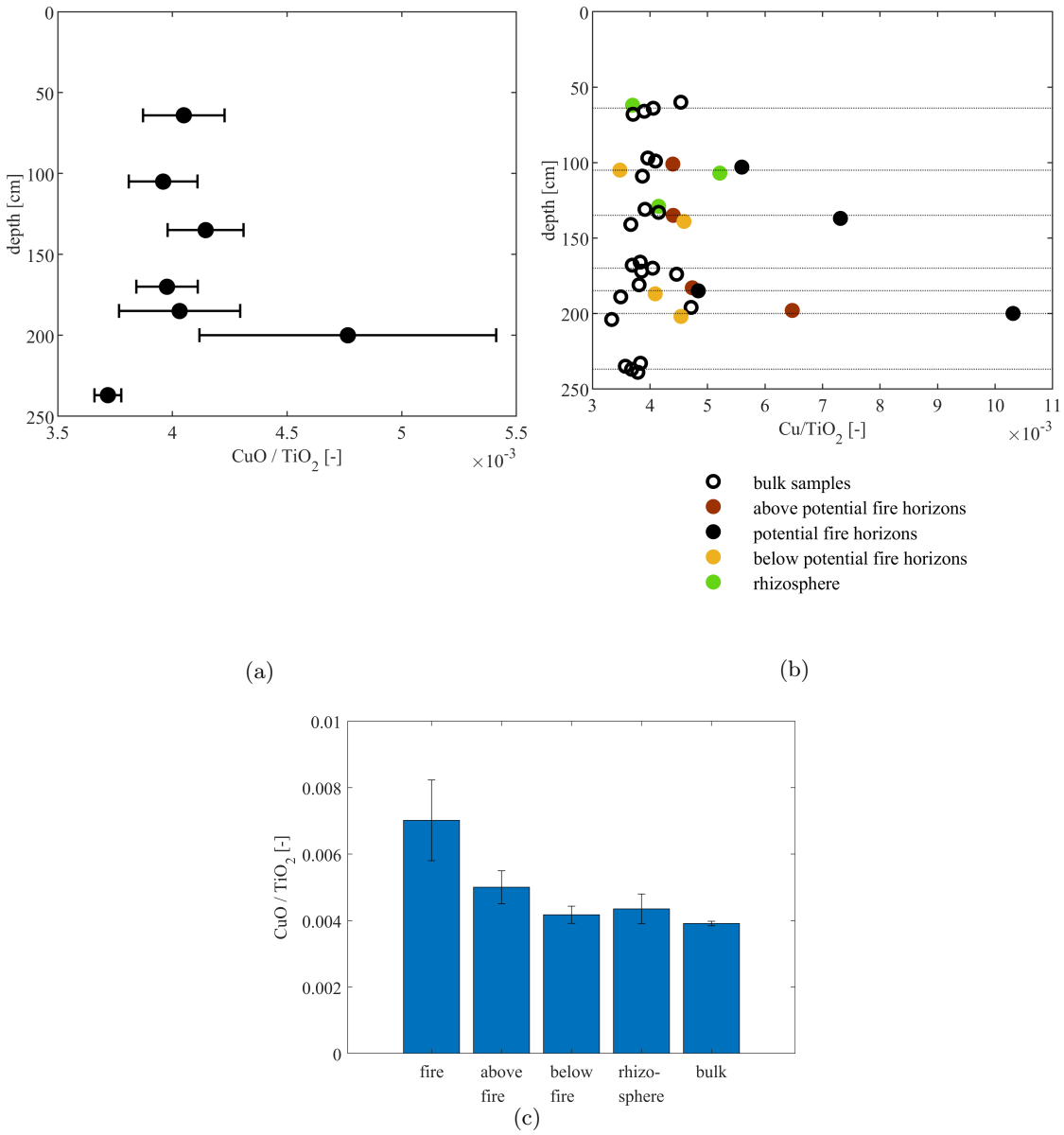

Figure C.27: The average normalized copper contents for each block with error bars representing the standard error of the mean are shown in (a). Picture (b) shows normalized copper contents for all samples. Fire horizons had higher CuO/TiO_2 contents than all other groups (c).

C.2 Total lipid extracts

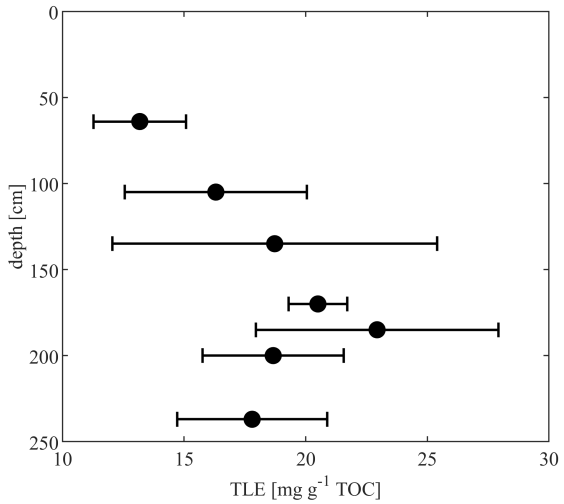

Figure C.28: The average TLE contents normalized to TOC for each block. Error bars represent the standard error of the mean.

C.3 Aliphatic hydrocarbons

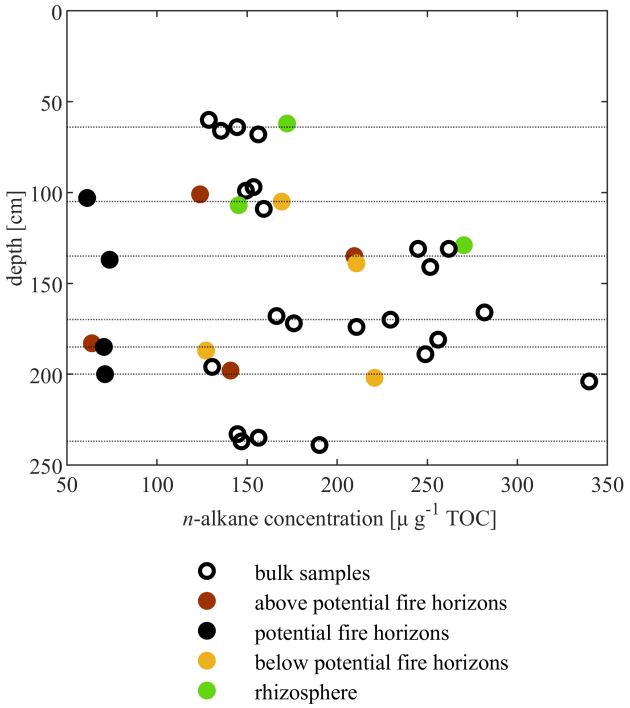

Figure C.29: *n*-alkane concentrations for all samples.

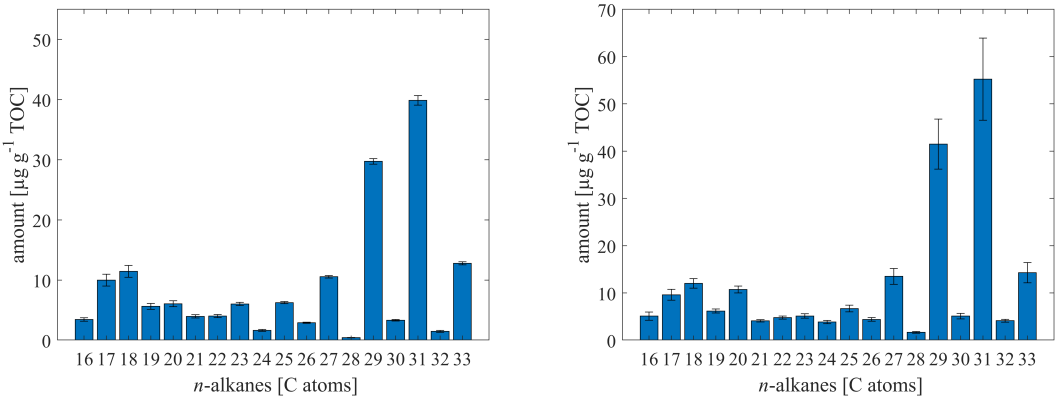

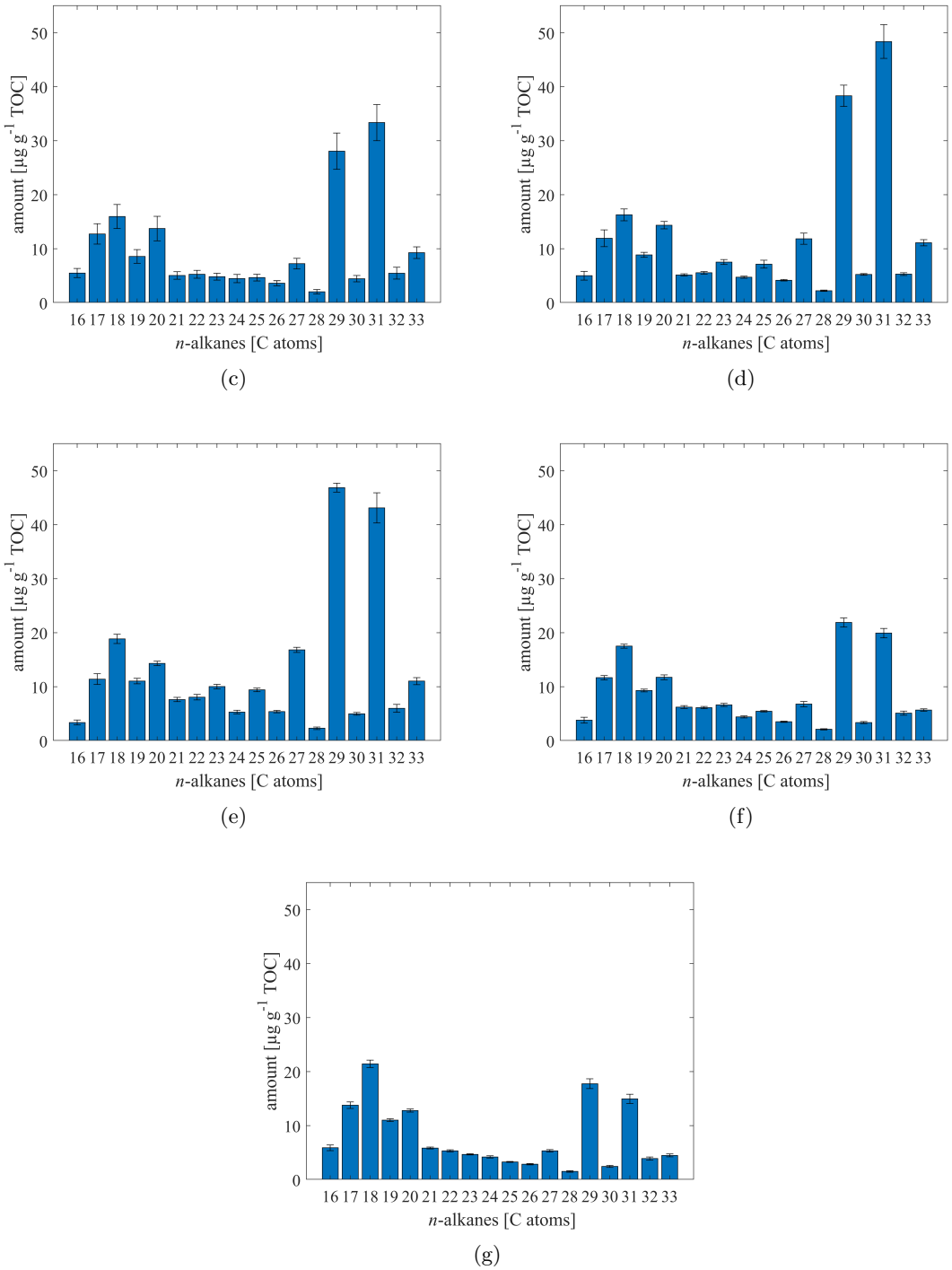

Figure C.30: The alkane distribution patterns for blocks 1 (a), 2 (b), 3 (c), 4 (d), 5 (e), 6 (f) and 7 (g) are shown. For each alkane the average was calculated. Fire horizons were excluded in an attempt to ensure that any depth dependent trend would not be masked by the sample type. Error bars represent the standard error of the mean.

C.4 BPCA

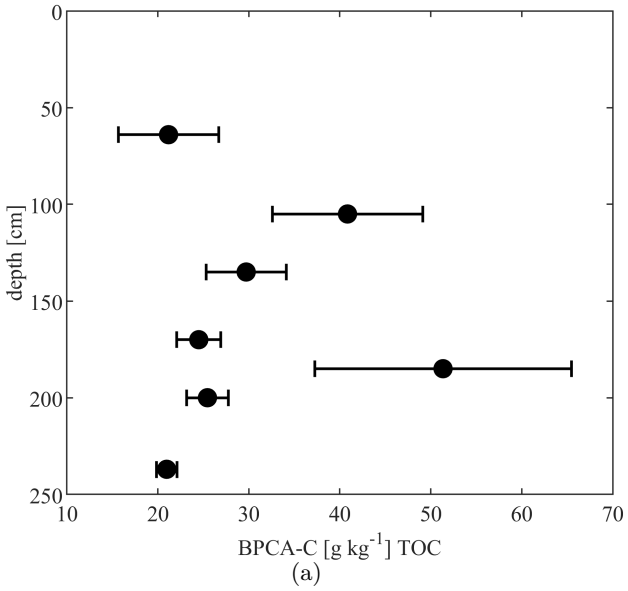

(a)

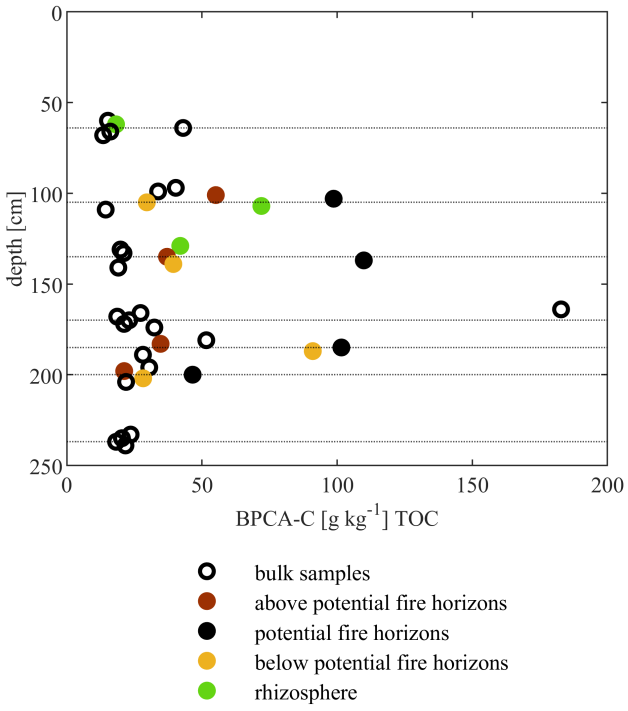

(b)

Figure C.31: The average BPCA-C contents for each block are shown in (a). Error bars represent the standard error of the mean. In (b) BPCA-C contents are plotted against the depth of the samples.

Personal declaration

I hereby declare that the submitted thesis is the result of my own, independent work. All external sources are explicitly acknowledged in the thesis.

Winterthur, April 29, 2020